Article

Mathematical Modeling and Validation of Glucose Compensation of the *Neurospora* Circadian Clock

Andrey A. Dovzhenok,[1] Mokryun Baek,[2] Sookkyung Lim,[1] and Christian I. Hong[2,*]
[1]Department of Mathematical Sciences, University of Cincinnati, Cincinnati, Ohio; and [2]Department of Molecular and Cellular Physiology, University of Cincinnati College of Medicine, Cincinnati, Ohio

ABSTRACT Autonomous circadian oscillations arise from transcriptional-translational feedback loops of core clock components. The period of a circadian oscillator is relatively insensitive to changes in nutrients (e.g., glucose), which is referred to as "nutrient compensation". Recently, a transcription repressor, CSP-1, was identified as a component of the circadian system in *Neurospora crassa*. The transcription of *csp-1* is under the circadian regulation. Intriguingly, CSP-1 represses the circadian transcription factor, WC-1, forming a negative feedback loop that can influence the core oscillator. This feedback mechanism is suggested to maintain the circadian period in a wide range of glucose concentrations. In this report, we constructed a mathematical model of the *Neurospora* circadian clock incorporating the above WC-1/CSP-1 feedback loop, and investigated molecular mechanisms of glucose compensation. Our model shows that glucose compensation exists within a narrow range of parameter space where the activation rates of *csp-1* and *wc-1* are balanced with each other, and simulates loss of glucose compensation in *csp-1* mutants. More importantly, we experimentally validated rhythmic oscillations of the *wc-1* gene expression and loss of glucose compensation in the $wc\text{-}1^{ov}$ mutant as predicted in the model. Furthermore, our stochastic simulations demonstrate that the CSP-1-dependent negative feedback loop functions in glucose compensation, but does not enhance the overall robustness of oscillations against molecular noise. Our work highlights predictive modeling of circadian clock machinery and experimental validations employing *Neurospora* and brings a deeper understanding of molecular mechanisms of glucose compensation.

INTRODUCTION

Circadian rhythms play a vital role in an organism's functions by anticipating daily changes in its environment. They influence various facets of organisms' activity including physiology, cell cycle, and metabolism. In the last two decades, experiments revealed that the core clock components used to construct the circadian oscillator are assembled as transcription-translation feedback loops (1,2) whose activity is modified through posttranslational modifications of the core components (3,4).

In *Neurospora crassa*, circadian timekeeping is sustained through interlocked negative and positive feedback loops. The WHITE COLLAR complex (WCC), a heterodimer of the zinc-finger proteins WC-1 and WC-2, activates the transcription of the *frequency* (*frq*) gene (5–7). Then, translated FREQUENCY (FRQ) protein binds to FRQ-interacting RNA Helicase and CK1 (3,8), translocates into the nucleus, and suppresses its own transcription by inactivating WCC, closing the negative feedback loop (9–11). Simultaneously, FRQ promotes WC-1 accumulation in the cytoplasm, increasing the level of WCC forming a positive feedback loop (12,13).

Recently, the circadian clock-regulated developmental regulator, *conidial separation-1* (*csp-1*) (14), was shown to be a global transcription repressor under the direct control of WCC, and was found to regulate expression of various metabolic and other genes (15). CSP-1 was shown to repress the expression of *wc-1* in a glucose-dependent manner by binding at the respective promoter (16) and forming an additional negative feedback loop. These intriguing findings illuminate a novel function of CSP-1 as an important regulator of the *Neurospora* core clock oscillator resembling that of REV-ERB-α/β in the mammalian circadian clock (17–19). Further experiments suggested that negative feedback via CSP-1 maintains relatively similar abundance of WC-1 in a wide range of glucose concentrations in the growth media. This results in a relatively constant circadian period as a function of glucose concentrations, which is referred to as "glucose compensation". In contrast, the glucose compensation was disrupted in $csp\text{-}1^{ko}$ with decreasing period with increasing glucose concentration (16).

In this article, we explore a *Neurospora* circadian clock model that includes CSP-1 as a newly identified element of the circadian system, and investigate molecular mechanisms for glucose compensation. Our model simulates glucose compensation of period by balancing the activation rates of *csp-1* and *wc-1* transcription, and loss of glucose

Submitted September 12, 2014, and accepted for publication January 9, 2015.

*Correspondence: christian.hong@uc.edu

Editor: James Keener.

0006-3495/15/04/1830/10 $2.00

http://dx.doi.org/10.1016/j.bpj.2015.01.043

compensation in *csp-1* mutants. Moreover, we predict and experimentally validate loss of glucose compensation in the *wc-1* overexpression (*wc-1*^{ov}) mutant. The model also accurately reproduces changes in clock period observed in previous experiments, and differential expression of FRQ and WC-1 in the nucleus versus cytoplasm (4,20).

Finally, it has been shown that the interlocked dual negative feedback loop increases oscillatory domain and possibly enhances the robustness of autonomous oscillations (21). We investigate robustness of the system against molecular stochasticity in the presence or absence of CSP-1 and show that a CSP-1-mediated negative feedback loop does not enhance the overall robustness of the system against molecular noise.

MATERIALS AND METHODS

Mathematical model of *Neurospora* circadian clock with CSP-1

The wiring diagram of the core oscillator and other ancillary components pertinent to this discussion is shown in Fig. 1. In the nucleus, nuclear WC-1 (WC-1$_n$) activates *frq* transcription with the rate constant k_1. FRQ protein is translated from *frq* mRNA in the cytosol and is translocated into the nucleus (processes with the rate constants k_2 and k_3, respectively). *frq* mRNA, cytosolic FRQ (FRQ$_c$), and nuclear FRQ (FRQ$_n$) degrade with the rate constants k_4, k_5, and k_6, respectively. The expression of *wc-1* is modeled with a maximum rate constant k_7, and the *wc-1* expression is modulated by the negative feedback from the global transcription repressor, CSP-1. Cytosolic WC-1 (WC-1$_c$) is translated and degraded with the rate constants k_8 and k_{10}, respectively. We assume that the accumulation of WC-1$_c$ is positively regulated by FRQ$_c$ (12). Then, WC-1$_c$ protein is either degraded (k_{11}) or translocated into the nucleus (k_9). We do not consider WC-2 in the model because WC-2 is present in excess of WC-1 and its concentration is relatively constant at all circadian times (6,7). Therefore, we consider the WCC complex to be represented in the model by WC-1$_n$. Finally, WC-1$_n$ starts *frq* transcription and then either slowly degrades (k_{12}) or is quickly inactivated (k_{13}/k_{14}) and degraded (k_{15}) via complex-formation with FRQ$_n$ closing the negative feedback loop.

Based on recent experimental findings (15,16), we extended the *Neurospora* circadian clock model (22) to include an additional negative feedback loop formed by the aforementioned transcriptional repressor, CSP-1. WC-1$_n$ starts transcription of *csp-1* (k_{16}), and the *csp-1* mRNA is degraded with the rate k_{17}. CSP-1 is translated and degraded with the rates k_{18} and k_{19}, respectively. We used the rate of degradation of CSP-1 from the previous experimental measurements (15). In the nucleus, CSP-1 inhibits the expression of *wc-1* as well as its own expression, as reported in Sancar et al. (15). In this study, we assume that the binding of CSP-1 to the *wc-1* promoter can be described by the Hill-type function similar to the one used to model inhibition of its own transcription in Sancar et al. (15).

The model includes the following rate equations:

$$\frac{d[frq\ \ \mathrm{mRNA}]}{dt} = k_1\frac{[\mathrm{WC\text{-}1_n}]^6}{K+[\mathrm{WC\text{-}1_n}]^6} - k_4[frq\ \ \mathrm{mRNA}] + k_{01},$$

$$\frac{d[\mathrm{FRQ_c}]}{dt} = k_2[frq\ \ \mathrm{mRNA}] - (k_3+k_5)[\mathrm{FRQ_c}],$$

$$\frac{d[\mathrm{FRQ_n}]}{dt} = k_3[\mathrm{FRQ_c}] + k_{14}[\mathrm{FRQ_n : WC\text{-}1_n}] - [\mathrm{FRQ_n}](k_6 + k_{13}[\mathrm{WC\text{-}1_n}]),$$

$$\frac{d[wc\text{-}1\ \ \mathrm{mRNA}]}{dt} = k_7\frac{K_1}{K_1+[\mathrm{CSP\text{-}1}]} - k_{10}[wc\text{-}1\ \ \mathrm{mRNA}] + k_{03},$$

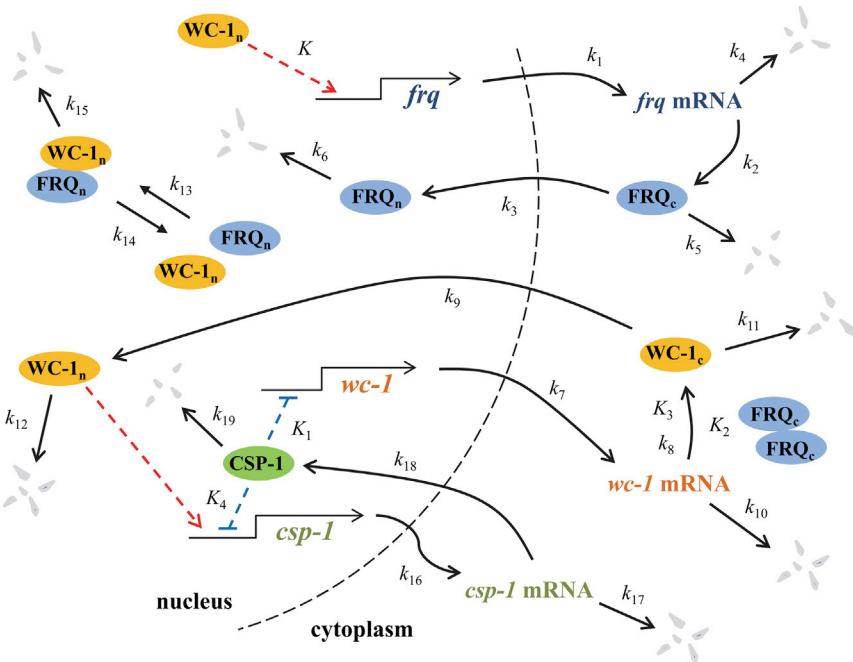

FIGURE 1 *Neurospora* clock model diagram with the global transcription repressor CSP-1. Transcriptional activator WC-1 starts transcription of the core clock gene *frq* whereas FRQ protein represses its own gene transcription in a negative feedback loop that promotes sustained circadian oscillations of core clock proteins. Transcriptional repressor CSP-1 inhibits *wc-1* gene expression forming another negative feedback loop in the model. (*Dashed arrows*) Activation, (*dashed lines* with *blunt ends*) repression via binding at the respective promoters. To see this figure in color, go online.

$$\frac{d[\text{WC-1}_\text{c}]}{dt} = k_8\frac{[\text{FRQ}_\text{c}]^2}{K_2+[\text{FRQ}_\text{c}]^2}\frac{[wc\text{-}1\ \ \text{mRNA}]}{K_3+[wc\text{-}1\ \ \text{mRNA}]} - (k_9+k_{11})[\text{WC}\ \ \text{-1}_\text{c}],$$

$$\frac{d[\text{WC-1}_\text{n}]}{dt} = k_9[\text{WC-1}_\text{c}] - [\text{WC-1}_\text{n}](k_{12}+k_{13}[\text{FRQ}_\text{n}]) + k_{14}[\text{FRQ}_\text{n}\text{: WC-1}_\text{n}],$$

$$\frac{d[\text{FRQ}_\text{n}\text{: WC-1}_\text{n}]}{dt} = k_{13}[\text{FRQ}_\text{n}]\times[\text{WC-1}_\text{n}] - (k_{14}+k_{15})[\text{FRQ}_\text{n}\text{: WC-1}_\text{n}],$$

$$\frac{d[csp\text{-}1\ \ \text{mRNA}]}{dt} = k_{16}[\text{WC-1}_\text{n}]\frac{K_4}{K_4+[\text{CSP-1}]} - k_{17}[csp\text{-}1\ \ \text{mRNA}]+k_{04},$$

$$\frac{d[\text{CSP-1}]}{dt} = k_{18}[csp\text{-}1\ \ \text{mRNA}]-k_{19}[\text{CSP-1}].$$

The parameter values are given in Table 1 (23–25). Parameters k_{01}, k_{03}, and k_{04} simulate additional transcription of corresponding genes to reproduce overexpression experiments with an inducible system, and have dimensions of a.u. h^{-1} and are initially set to zero. Concentrations in arbitrary units (a.u.) reflect the number of molecules per unit volume. Experimentally measured rate constants are indicated in Table 1. The rest of the rate constants have been chosen to fit the model to experimental data simulating the abundance of total and nuclear WC-1 and FRQ, and the period change observed in *frq*, *wc-1*, and *csp-1* overexpression experiments in wild-type (WT) and mutant strains.

Justifications of the model

In this study, we use a relatively high cooperativity ($n = 6$) of WC-1_n binding at the *frq* promoter. This high cooperativity is necessary to increase nonlinearity in our simple model to simulate the existing experimental data on changes in period in clock overexpression mutants (see Fig. 3 and Text S1 in the Supporting Material for more details). In our model, we do not include posttranslational modification such as progressive phosphorylation of FRQ (26) or the coiled-coil domain-mediated FRQ-FRQ interaction (4) to reduce the complexity of the model while simulating existing molecular phenotypes. If they are included in the model, they may increase overall nonlinearity of the system and allow for a lower Hill coefficient of WC-1_n activation of *frq* transcription. However, this would make the model significantly more complex and, therefore, we do not include them in this simple model. See also Text S1 in the Supporting Material for further discussion. Also, we assume that the accumulation of WC-1_c shows saturation kinetics with reference to *wc-1* mRNA. This saturation behavior, although not reported experimentally, may occur due to FRQ-promoted accumulation of WC-1_c as we showed before in Hong et al. (22) and allows the model to reproduce experimental data on *wc-1* overexpression (see Fig. 3, *B* and *C* and Text S1 for more details).

Lastly, in our stochastic simulations, we used standard Michaelis-Menten and Hill-type functions (Table S1 in the Supporting Material) derived via quasi-steady-state approximation instead of a large number of elementary reactions. This approach, resulting in a compact model description, was studied before in a circadian clock model (27) and other systems (28) and was shown to produce satisfactory agreement between detailed and compact models. The compact models are favorable because the actual molecular mechanisms that comprise Hill-type and Michaelis-Menten functions are usually unknown. However, recent studies have found that stochastic simulations of the compact model are not always accurate (29–31). We confirm validity of our stochastic simulation results produced with the Gillespie algorithm by rewriting the model as Langevin-type equations with additive or multiplicative noise (32) and obtaining qualitatively similar results (see Figs. 7 and S9).

TABLE 1 Parameter values for the *Neurospora* clock model

Parameter	Value	Dimension	Parameter	Value	Dimension
k_1	1.8	a.u. h^{-1}	k_{13}	50	$(\text{a.u.})^{-1}\ h^{-1}$
k_2	1.8	h^{-1}	k_{14}	1	h^{-1}
k_3	0.05	h^{-1}	k_{15}	5	h^{-1}
k_4 (23)	0.23	h^{-1}	k_{16}	0.12	h^{-1}
k_5 (24)	0.27	h^{-1}	k_{17}	1.4	h^{-1}
k_6 (24)	0.27	h^{-1}	k_{18}	50	h^{-1}
k_7	0.5	a.u. h^{-1}	k_{19} (15)	1.4	h^{-1}
k_8	1	a.u. h^{-1}	K	1.25	$(\text{a.u.})^6$
k_9	40	h^{-1}	K_1	3	a.u.
k_{10} (25)	0.1	h^{-1}	K_2	1	$(\text{a.u.})^2$
k_{11}	0.05	h^{-1}	K_3	10	a.u.
k_{12}	0.02	h^{-1}	K_4	3	a.u.

Experimentally measured rate constants are followed by a reference.

Computer simulations

We used XPPAUT software (Bard Ermentrout, University of Pittsburgh, http://www.math.pitt.edu/bard/xpp/xpp.html) to obtain numerical solutions, bifurcation, and period diagrams of the model equations.

Stochastic simulations

Stochastic simulations were carried out in MATLAB (The MathWorks, Natick, MA) by utilizing the Gillespie algorithm (33,34). We assigned the probability of occurrence of a particular reaction to each term of the kinetic model as shown in Table S1. The Gillespie algorithm then randomly chooses the reaction that occurs at each time step according to its probability and the time interval to the next reaction step. The number of molecules and the reaction probabilities are then updated at each time step according to Table S1. Parameter Ω in the Gillespie method allows modulation of the strength of noise in the stochastic model formulation by controlling the number of molecules that are present in the system. Each simulation was run for 3000 h and we removed the first 500 h to allow for transients to subside.

Strains

Strains used for the experiments are a clock wild-type *ras-1*^{bd} (328-4), *wc-1-luc::csr-1*, and *wc-1*^{ov};*frq-luc::his-3*. The strain *wc-1-luc::csr-1* was created by integrating the *wc-1* promoter with a codon-optimized firefly luciferase into the *csr-1* locus as previously described in Chen et al. (35) in a clock wild-type *ras-1*^{bd} (328-4). The strain *wc-1*^{ov} was created by integrating a *wc-1* open reading frame with its endogenous promoter into the *csr-1* locus as previously described in Chen et al. (35) in the strain containing *frq-luciferase* reporter (36).

Western blot

Neurospora were grown in liquid culture media containing Vogel's medium (pH 5.8) with either 0.1% or 0.3% glucose, 0.5% arginine, 50 ng/mL biotin,

and harvested at indicated time points. Immunoblot analysis was performed as previously described in Garceau et al. (26) except that we used 1) 20 μg of protein per lane, 2) 6.5% sodium dodecyl sulfate-polyacrylamide gel electrophoresis, 3) anti-WC-1 or anti-FRQ (1:300) as primary antibody, and 4) goat anti-rabbit IgG (H+L) (1:5000, No. 170-6515; Bio-Rad, Hercules, CA) as secondary antibody.

Race tube and bioluminescence assays

Race tube and bioluminescence assays were performed as previously described in Hong et al. (37) and Dunlap and Loros (38). We used standard race tubes containing Vogel's medium (pH 5.8) with 0.17% arginine, 50 ng/mL biotin, 1.5% agar, and 12.5 μM of luciferin for bioluminescence assays, and varying concentrations of glucose (0.1–0.3% m/v).

RESULTS

The proposed circadian clock model reproduces wild-type and mutant phenotypes

Fig. 2, *A–C*, shows oscillation profiles derived from the simulated WT circadian system and Fig. 2 *D* shows experimental data from the *wc-1-luciferase* reporter.

The abundance of total FRQ is greater than the abundance of total WC-1 (20), and there is 4–10 h of phase difference between FRQ and WC-1 depending on whether we measure by the peak or trough of the protein concentrations (Fig. 2 *A*) (12). In contrast to total WC-1 and FRQ concentrations, $WC\text{-}1_n$ levels are higher than FRQ_n levels because FRQ is mainly localized in the cytoplasm (4,20), which is also simulated in our model (Fig. 2 *B*). Negative feedback from CSP-1 onto *wc-1* expression is moderate, resulting in low-amplitude oscillations of *wc-1* mRNA levels (Fig. 2 *C*) that were not reported previously. Oscillations of *wc-1* mRNA may not have been observed in previous experiments (12) due to their low amplitude and the presence of molecular noise. We constructed a *wc-1* bioluminescence reporter by fusing the promoter of *wc-1* with a codon-optimized firefly luciferase, and validated that gene expression of *wc-1* oscillates in a circadian manner (Fig. 2 *D*). Garceau et al. (26) observed a rapid rise in *frq* mRNA level and its subsequent rapid exponential decay. In contrast, the increase in FRQ protein concentration was followed by a slower, almost linear decay of FRQ protein level (26). In the model, the temporal profiles of *frq* mRNA (Fig. 2 *C*) and total FRQ protein (Fig. 2 *A*) accurately reproduce these distinct shapes of *frq* mRNA and FRQ protein oscillations. The expression of *csp-1* shows circadian oscillations with peak expression aligned with the peak of WC-1 (WCC) because its expression is controlled by WCC (14,15) (Fig. 2 *C*).

Our model not only reproduces wild-type profiles, but also simulates experimentally observed changes in period in different clock overexpression strains. In *Neurospora*, the quinic acid (QA)-inducible system is readily used to increase the expression of a target gene in a QA dosage-dependent manner (39,40). Use of this for *frq* overexpression (*frq*$^+$;*qa-2-frq*) results in small changes in period at low induction, and abolishes oscillations at high induction (40). In Fig. 3 *A*, we show that overexpression of *frq* with parameter k_{01} that simulates additional transcription of the *frq* gene (see model equations in Materials and Methods) does not produce large changes in period, and the system transitions into a stable steady state with no oscillations when the value of k_{01} is >0.14. It is important to note that

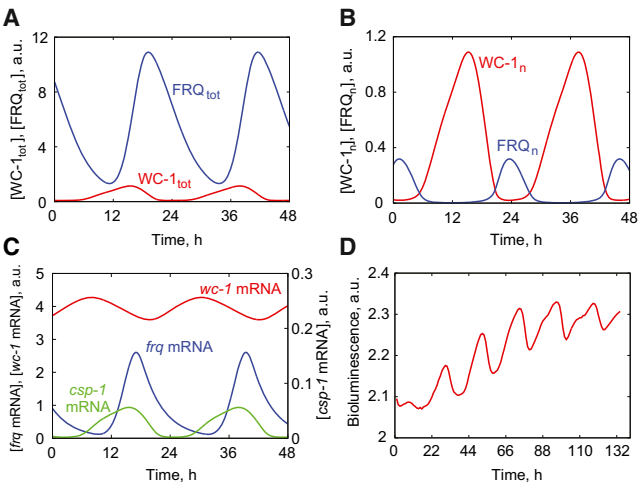

FIGURE 2 Oscillatory profiles for the wild-type parameterization. (*A*) Total WC-1 and FRQ levels show greater abundance of FRQ compared to WC-1. (*B*) The abundance of $WC\text{-}1_n$ is greater than FRQ_n for the most of circadian time. (*C*) All three transcripts of *frq*, *wc-1*, and *csp-1* show sustained oscillations. (*D*) The *wc-1-luciferase* reporter shows robust circadian oscillations as predicted in the model. This data is a representative of three independent experiments. Arbitrary units (a.u.) are shown. To see this figure in color, go online.

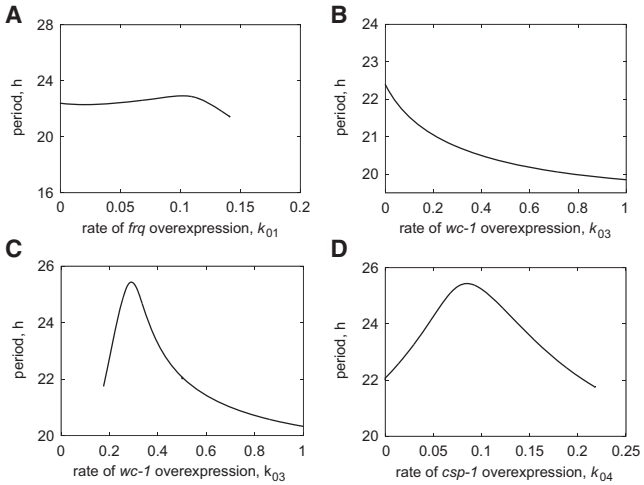

FIGURE 3 The model reproduces overexpression phenotypes of *frq*, *wc-1*, and *csp-1*. (*A*) Clock period as a function of the rate of *frq* overexpression, k_{01} in wild-type genetic background. (*B*) Clock period as a function of *wc-1* overexpression rate, k_{03}, in wild-type genetic background. (*C*) Clock period as a function of *wc-1* overexpression rate, k_{03}, in *wc-1*^{ko} genetic background (the *wc-1* expression rate constant $k_7 = 0$). (*D*) Clock period as a function of k_{04}, simulating the rate of *csp-1* overexpression in *qa-2* promoter knock-in experiment (the *csp-1* expression rate constant $k_{16} = 0$).

the amplitude of FRQ_n plays a critical role in determining the period of the system (Fig. S1 in the Supporting Material). The period is maintained in the case of *frq* overexpression, because there is only a minimal change in the amplitude of FRQ_n oscillations before the system transitions to a stable steady state crossing a Hopf bifurcation point (Fig. S2).

On the other hand, *wc-1* overexpression (*wc-1*$^+$;*qa-2-wc-1*) experiments reveal a monotonically decreasing period with increasing concentration of the inducer, QA (6). This decrease of period is observed as a function of the rate of *wc-1* overexpression, k_{03} (Fig. 3 *B*). Cheng et al. (6) also performed overexpression of *wc-1* in the *wc-1*^{ko} background (*wc-1*^{ko};*qa-2-wc-1*), and observed no oscillations at low QA levels. However, the period decreased from ~24.5 h to 22.8 h at higher QA levels (6). Our model reproduces experimentally observed shortening of the period with the increase in *wc-1* overexpression rate k_{03} in a simulated *wc-1*^{ko} strain ($k_7 = 0$) (Fig. 3 *C*). The initial transient increase of the period in the model (Fig. 3 *C*) corresponds to the parameter range near the Hopf bifurcation that is characterized by low albeit increasing amplitude of FRQ_n oscillations (Fig. S3 and see Text S2 in the Supporting Material for the mechanism of period regulation), which are easily destroyed in the model in the presence of molecular noise (Fig. S4).

In contrast to the decrease of period with *wc-1* overexpression, Sancar et al. (15) observed an increase of period by ~2.5 h with a moderate overexpression of *csp-1*, and then a loss of circadian rhythms with higher induction of *csp-1* in a *csp-1*^{ko} background (*csp-1*^{ko};*qa-2-csp-1*) (15). Our model reproduces period lengthening of the circadian clock with the increase of *csp-1* expression as modeled by increasing the rate of *csp-1* overexpression, k_{04}, in the *csp-1*^{ko} background ($k_{16} = 0$) (Fig. 3 *D*). The increase of period coincides with the rapid decrease in FRQ_n levels (Fig. S5, *A* and *B*, and see Text S2 in the Supporting Material). Interestingly, FRQ_c levels decrease more gradually than FRQ_n (Fig. S5 *B*). Finally, a decrease in period occurs in the model for larger values of k_{04} (Fig. 3 *D*). This period decrease is characterized by low abundance of FRQ_n (Fig. S5 *B*) that is no longer able to effectively clear WC-1 from the nucleus so that the amplitude of $WC\text{-}1_n$ oscillations becomes small (Fig. S5 *C*). These low-amplitude oscillations are likely to be destroyed by molecular noise (see Fig. S4) and, therefore, may not be observed experimentally (16). This conclusion is indirectly suggested by a strongly damped amplitude of *frq-luc* bioluminescence as well as weakened conidiation rhythm observed at an intermediate QA level right before the loss of circadian oscillations in *csp-1* overexpression experiments (16). It is important to note that the increase in *csp-1* overexpression (k_{04}) corresponds to the decrease of *wc-1* overexpression rate, k_{03}, because of the repression CSP-1 exerts on *wc-1* transcription. Hence, the decrease of period observed in Fig. 3 *D* is equivalent to the increase of period shown in Fig. 3 *C*.

Point mutations of *frq* that alter the circadian period have been interpreted as changing the half-life of the FRQ protein (41,42). Experimental (24,43) and modeling (23,44) studies are consistent with this, showing a strong correlation between FRQ stability and the period of the clock, with slow FRQ degradation (*frq*^{7}) seen with longer periods whereas fast degradation of FRQ (*frq*^{1}) is seen with shorter periods. Our model simulates periods of *frq*^{1} and *frq*^{7} mutants by changing the FRQ degradation rate constant (Fig. S6), which is consistent with previous results.

The glucose compensation is achieved by balancing the rates of activation between *frq* and *csp-1*

The period of circadian rhythms is relatively insensitive to changes in nutrient conditions. As demonstrated in recent experiments, *Neurospora crassa* showed small changes in period over a wide range of glucose concentrations (16). In contrast, a significantly shorter period was observed in *csp-1*^{ko} compared to WT with increasing glucose levels (16). In the same study, an increased abundance of *wc-1* mRNA and WC-1 were observed in *csp-1*^{ko} compared to WT in high-glucose (2%) but not in low-glucose (0.1%) conditions. On the other hand, a glucose-dependent increased level of CSP-1 was observed in *wc-2*^{ko} (16), which suggested that glucose-induced expression of CSP-1 is independent of WCC. The glucose-dependent repression of *wc-1* transcription by CSP-1 strongly suggests a central role of CSP-1 in a circadian glucose compensation mechanism. This led Sancar et al. (16) to hypothesize that glucose compensation of the circadian period is achieved by balancing increased abundance of WC-1 with the CSP-1-dependent repression of *wc-1* transcription.

To begin with, we simulated the *csp-1*^{ko} strain by setting the rate constant of *csp-1* expression $k_{16} = 0$. We modeled different glucose levels by changing the rate constant of *wc-1* expression, k_7, according to the reported increase in WC-1 protein abundance at high glucose concentrations (16). Our model reproduces the decrease of period as a function of the rate of *wc-1* transcription (k_7) (Fig. 4 *A*). The decrease in period is accompanied by an increase in FRQ_n amplitude (Fig. 4 *B* and see Text S2 in the Supporting Material), whereas the saturation of FRQ_n and $WC\text{-}1_n$ amplitudes (Fig. 4, *B* and *C*) corresponds to the stabilization of the period at ~20 h (Fig. 4 *A*). There exists a narrow region where the period sharply increases with increasing rate constant k_7 (Fig. 4 *A*). This region corresponds to low-amplitude oscillations near Hopf bifurcation (Fig. 4, *B* and *C*) that are easily destroyed by molecular noise (see Fig. S4).

To investigate glucose compensation with our model, we computed the constant period curves in the two-parameter bifurcation plane of the rates of *csp-1* (k_{16}) and *wc-1* (k_7)

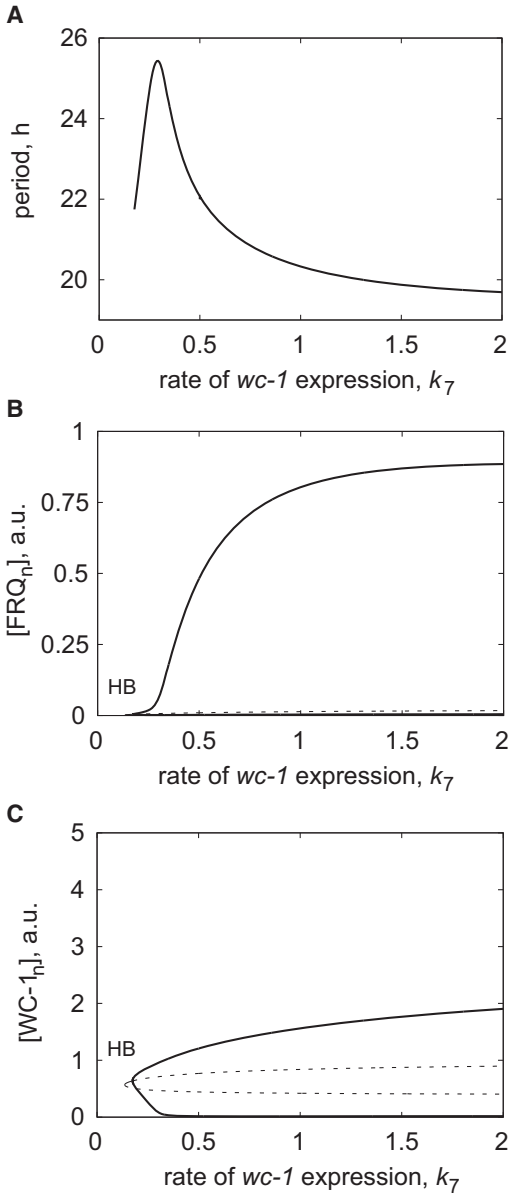

FIGURE 4 Simulated loss of glucose compensation of circadian clock in the *csp-1*^{ko} strain. (*A*) Clock period as a function of parameter k_7, simulating the increase in glucose concentration. One-parameter bifurcation diagrams show the envelopes (maximum and minimum) of (*B*) FRQ_n and (*C*) $WC\text{-}1_n$ oscillations as a function of k_7. Oscillatory region is bounded by supercritical Hopf bifurcation (*HB*) at low values of k_7 and is unbounded at high values of k_7 due to saturation of WC-1 synthesis with respect to *wc-1* mRNA (see Materials and Methods). (*Thick solid curves*) Stable oscillatory solutions; (*thin solid curves*) stable steady states; (*dashed curves*) unstable steady states. The rate of synthesis of *csp-1* mRNA is set to zero ($k_{16} = 0$) for these simulations.

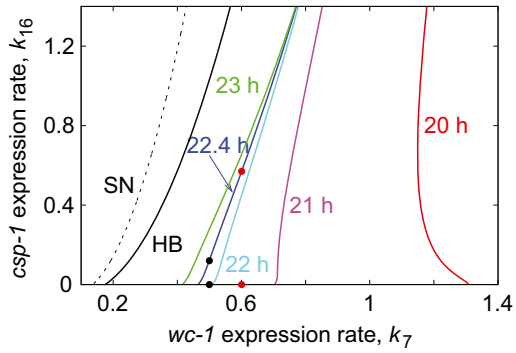

FIGURE 5 Simulated glucose compensation of the clock period in wild-type and its loss in *wc-1*^{ov} mutant. The two-parameter bifurcation diagram in *wc-1* and *csp-1* transcription rate constants k_7 and k_{16}, correspondingly, shows curves of constant period, color-coded. Oscillatory solutions appear from the Hopf bifurcation (*HB*). Parameter sets in low-glucose (*black dots*) and high-glucose (*red dots*) conditions are used for stochastic simulations in the analysis of period robustness against molecular stochasticity. The *csp-1*^{ko} corresponds to the x axis in the diagram ($k_{16} = 0$). The values of the model parameters are as described in Materials and Methods.

transcription (Fig. 5). Our analysis demonstrates that fixed period curves have a remarkably constant positive slope around the wild-type period of ~22.4 h. Hence, simultaneous increase of the above pair of parameters leads to a constant period in the model. The shorter period with an increase of *wc-1* transcription rate as a function of glucose concentration is compensated near the WT period by the longer period with the increase of *csp-1* transcription rate, which results in the repression of *wc-1* expression by the increased amount of CSP-1 (16). Therefore, our model is consistent with the glucose compensation being achieved by balancing the synthesis of *wc-1* and *csp-1*.

Intriguingly, the fixed period curve for a short period ($T = 20$ h) at higher values of k_7 has a negative slope (Fig. 5). Near the period $T = 20$ h ($k_7 = 1.2$), increase of *csp-1* expression rate (k_{16}) results in a shorter period, which is the opposite behavior to when the system is in the wild-type regime ($k_7 = 0.5$). In other words, the balance between *wc-1* and *csp-1* transcription that we observe near the WT period $T = 22.4$ h is no longer present in a different parameter space with a period $T = 20$ h. Therefore, the *wc-1* expression rate has to decrease to maintain constant period, which results in the negative slope of the fixed period curve $T = 20$ h (Fig. 5).

Based on this analysis, our model predicts a loss of glucose compensation in a *wc-1* overexpression mutant (i.e., increased rate of *wc-1* transcription) if we assume that both *csp-1* and *wc-1* synthesis rates increase as a function of glucose concentration in the growth media. To test this hypothesis, we constructed a *wc-1* overexpression strain by transforming an additional *wc-1* gene with its endogenous promoter at the *csp-1* locus into a *Neurospora* strain that contains a *frq-luc* bioluminescence reporter (36). WC-1 protein abundance is increased in the *wc-1*^{ov} strain compared to the wild-type (Fig. 6 *A*). More importantly, the *wc-1*^{ov} strain demonstrates a decrease of period as a function of glucose concentration in both race tube (Fig. 6, *B* and *C*) and *frq-luciferase* bioluminescence assays (Fig. 6 *D*); these data indicate a loss of glucose compensation.

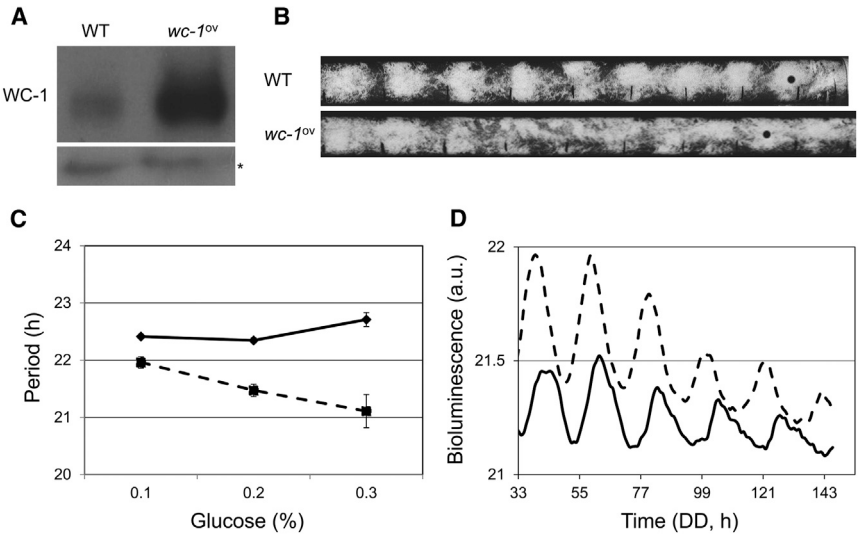

FIGURE 6 Loss of glucose compensation in the *wc-1*^{ov} mutant. (*A*) Western blot shows increased abundance of WC-1 in the *wc-1*^{ov} mutant. Nonspecific bands (*) are shown as a loading control. This is a representative blot from three experiments. (*B*) Representative race tubes of wild-type and the *wc-1*^{ov} mutant grown on a defined agar media (see Materials and Methods) with 0.3% glucose (m/v). (*Small black bars*) Markings of *Neurospora* growth front in every 24 h. (*Black dots* on the race tubes) Period of *wc-1*^{ov} is shorter than the wild-type. (*C*) Graph showing free running periods from wild-type (*solid line*) and *wc-1*^{ov} (*dashed line*) in the media containing different glucose concentrations. The period decreases in *wc-1*^{ov} with increasing glucose concentration in the media. The periods of race tube assay of the wild-type are 22.41 $\pm$ 0.03 h at 0.1% glucose, 22.35 $\pm$ 0.04 h ($n = 6$) at 0.2% glucose, and 22.71 $\pm$ 0.12 h ($n = 6$) at 0.3% glucose. The quantified periods of race tube assay of the *wc-1*^{ov} at different glucose concentrations are 21.96 $\pm$ 0.1 h ($n = 6$) at 0.1% glucose, 21.47 $\pm$ 0.11 h ($n = 6$) at 0.2% glucose, and 21.11 $\pm$ 0.3 h ($n = 5$) at 0.3% glucose. Error bars represent mean $\pm$ SE. (*D*) Graph showing bioluminescence activity from *frq-luciferase* reporter from wild-type (*solid curve*, 21.82 h) and *wc-1*^{ov} (*dashed curve*, 20.87 h). *Neurospora* are grown in the media containing 0.3% glucose (m/v). *wc-1*^{ov} demonstrates shorter period compared to wild-type, which is consistent with (*B*). The figure shows a representative data from three independent experiments.

Analysis of period robustness against molecular stochasticity

It has been shown that the interlocked dual negative feedback loop creates a wider oscillatory domain (21). We wondered if the additional negative feedback loop mediated by CSP-1 enhances the robustness of the system against molecular noise as a function of glucose concentration. To test this hypothesis, we performed stochastic simulations of the clock model to determine the effect of noise on the period of *Neurospora* circadian oscillator in both WT and *csp-1*^{ko} as a function of glucose concentration (i.e., low and high values of k_7 and k_{16}). The period histograms of stochastic simulations in low-glucose conditions (*black dots* in Fig. 5) are plotted in Fig. 7. In the case of a strong noise, the WT parameter set shows larger variation of the periods (Fig. 7 *A*) when compared to the period variation in the case of the *csp-1*^{ko} parameter set (Fig. 7 *B*). In the case of a weak noise, we observed similar behavior except period variation was smaller, as expected for weak noise (Fig. S7, *A* and *B*). Therefore, unexpectedly, *csp-1*^{ko} appears to be slightly more robust than the WT with either strong or weak noise in the system.

We also investigated the effect of noise in the model in high glucose conditions (*red dots* in Fig. 5). Here, similar to low-glucose conditions, the WT had more variation in period compared to *csp-1*^{ko} when strong noise was present (Fig. 7, *C* and *D*). Notably, the WT in high glucose had similar period sensitivity compared to the WT in low glucose (Fig. 7, *C* and *A*), whereas *csp-1*^{ko} in high glucose had less variation in period compared to *csp-1*^{ko} in low glucose (Fig. 7, *D* and *B*). In the case of weak noise, period variation in WT and *csp-1*^{ko} in high glucose resembled the results in the case of strong noise (Fig. S7, *C* and *D*) as well as between high- and low-glucose parameter sets (Fig. S7), but variation of periods was smaller as expected for weak noise. The race tube and bioluminescence data show a robust circadian period with standard errors at ~0.2 h or 10% even in the *csp-1*^{ko}, which is consistent with our simulations (16).

It is important to note that the location of the WT parameter space is closer to the Hopf bifurcation compared to *csp-1*^{ko} parameter space (Fig. 5), because it was previously shown that the proximity of a Hopf bifurcation leads to less robust oscillations against noise (45). Therefore, to make a fair comparison of robustness of *csp-1*^{ko} and WT parameter sets against noise, we performed stochastic simulations of the *csp-1*^{ko} parameter set in very low glucose (Fig. S8) that has a similar distance to Hopf bifurcation as the WT parameter set in low glucose. We observed period variation that was similar to the WT parameter set (Figs. S8 and 7), which indicates that the proximity to the Hopf bifurcation plays a defining role in determining the robustness of circadian oscillations against noise in the *Neurospora* clock.

DISCUSSION

In this article, we constructed a mathematical model of the *Neurospora* circadian clock that incorporates a transcriptional repressor, CSP-1 (15), which resulted in a model with interlocked dual negative feedback loops (Fig. 1). This network topology resembles the mammalian circadian clock model in which REV-ERB-α/β forms a second

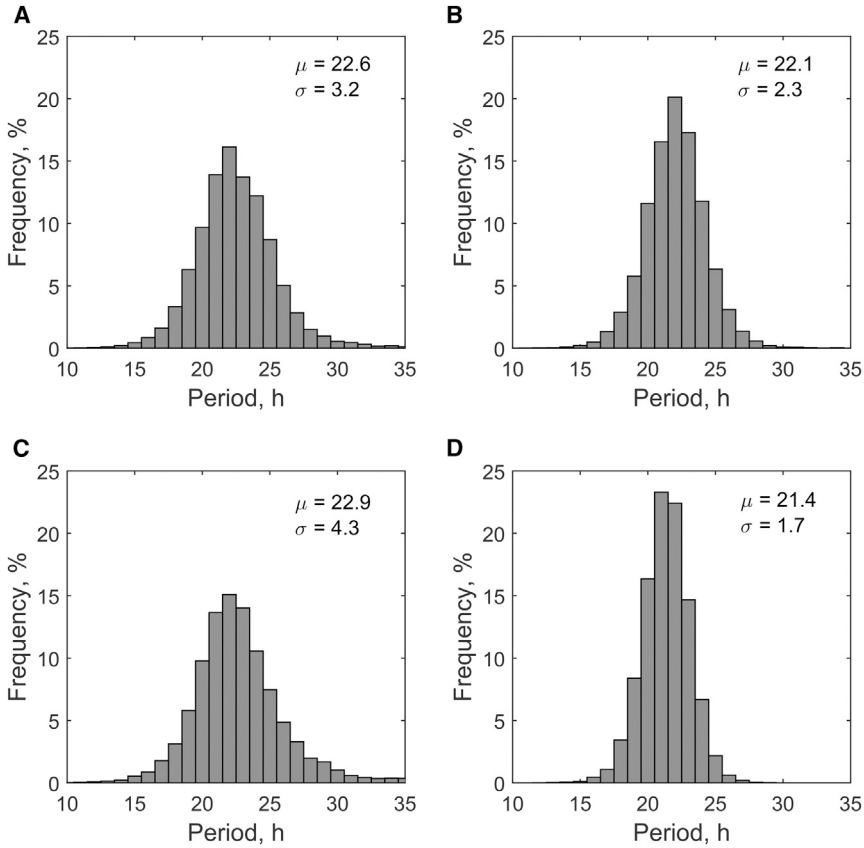

FIGURE 7 Histograms of period distributions obtained by stochastic simulations with strong noise. Period distribution in the presence of strong noise for the WT (*A* and *C*) and *csp-1*^{ko} (*B* and *D*) in low and high glucose, correspondingly. The histograms of periods of 10,000 cycles were computed from 100 simulation runs with 100 successive cycles with the volume factor $\Omega = 100$. The period was determined as the time interval separating two successive peaks of FRQ_c. The mean value (μ) and standard deviation (σ) of the period (in hours) is shown in each histogram. Parameter values are as described in Materials and Methods, except (*B*) $k_{16} = 0$, (*C*) $k_7 = 0.6$, $k_{16} = 0.57$ and (*D*) $k_7 = 0.6$, $k_{16} = 0$.

negative feedback loop inhibiting the circadian clock transcription factor, CLOCK/BMAL1 (21). The model simulates the changes in clock period observed in different overexpression experiments (Fig. 3). Moreover, the model accurately reproduces compensation of clock period across glucose concentrations (Fig. 5) and the loss of this compensation in *csp-1* mutants (Fig. 4 *A*). Glucose compensation in the model is achieved by balancing the rates of *wc-1* and *csp-1* transcription. This balance is lost in the *csp-1* mutant and the period of the clock decreases at high glucose concentration in the media. Our model predicts the loss of glucose compensation in *wc-1*^{ov} mutants (Fig. 5), which indicates that glucose compensation is achieved within a narrow range of parameter space. More importantly, we validate this modeling prediction in experiments (Fig. 6).

Based on our data and the similarities in the regulatory architecture of the fungal and animal circadian clocks (1,46), we hypothesize defective glucose compensation in *Clk* and *Bmal1* overexpression mutant mice. The outcome of this hypothesis will depend on how glucose influences the master clock in the suprachiasmatic nucleus, which coordinates peripheral clocks (47). It has been shown that high-fat diet shifts patterns of mouse food intake and attenuates amplitudes of clock components (48). Similarly, it would be interesting to investigate glucose-dependent changes of phase and amplitude of core circadian clock components in *Neurospora*, and the function of CSP-1 in such responses. Furthermore, it will be critical to investigate the range of glucose compensation and interconnected molecular responses of circadian rhythms and glucose metabolism to determine the glucose metabolism-dependent physiological outcomes.

The robustness of an oscillatory system against molecular noise depends on several factors including the network topology, parameter space, and functions. Recently, several studies investigated the effect of the second negative feedback loop on robustness of the negative feedback oscillatory systems (21,49). Tsai et al. (49) reported no improvement from additional negative feedback in oscillatory range or operational frequency range for simple oscillator models in accord with our findings for the *Neurospora* clock. In contrast, Kim and Forger (21) showed that the additional slow negative feedback loop on the core clock oscillator increases the oscillatory range of the system. More importantly, they also demonstrated that the second negative feedback loop regulates stoichiometric balance of core clock repressors and activators that is critical for sustained oscillations. However, the second negative feedback loop formed by CSP-1 in *Neurospora* is fast relative to the core negative feedback loop (the ratio of *csp-1* mRNA degradation rate to *frq* mRNA degradation rate $\delta \approx 6$). Both the *Neurospora* clock and the model of Tsai et al. (49) include

Hill functions to describe transcription, whereas the model of Kim and Forger (21) uses protein sequestration. A recent study also showed how models behave differently depending on the choice of transcriptional mechanism between protein sequestration and Hill functions (50). Therefore, our study provides further confirmation for the hypothesis that the effect of an additional negative feedback loop on robustness of the system may depend on the mechanism of transcriptional regulation in the model.

Our stochastic simulations revealed that a CSP-1-mediated negative feedback loop does not enhance robustness of the oscillatory system against noise, because the robustness of the circadian oscillator strongly depends on the proximity of the system to the Hopf bifurcation (Figs. 5 and 7), which is in agreement with previous modeling results (21,45). In particular, in the model of Kim and Forger (21), the second negative feedback loop increases the oscillatory range and, thus, increases the distance of the system to the Hopf bifurcation. Moreover, our simulations indicate that the oscillations are quickly lost even in the presence of a weak molecular noise when the system is in immediate vicinity of the Hopf bifurcation (Fig. S4). These modeling results are confirmed by experimental data on *wc-1* overexpression in *wc-1*^{ko} background (6) and on *csp-1* overexpression in *csp-1*^{ko} background (16). These experimental data show weak and fragile conidiation rhythm, reduced amplitude of *frq* bioluminescence, and increased standard errors of circadian periods right after the appearance of oscillations or just before losing their rhythmicity, which strongly suggests loss of robustness of circadian clock against molecular noise near transitions to steady states. In this report, we demonstrate that iterative mathematical modeling and experimental validations advance our detailed understanding of the *Neurospora* circadian system, and continued development of such models will elucidate interconnected molecular responses between the circadian clock and glucose metabolism.

SUPPORTING MATERIAL

Supporting Materials and Methods, 12 figures, and one table are available at http://www.biophysj.org/biophysj/supplemental/S0006-3495(15)00222-2.

ACKNOWLEDGMENTS

We thank H. Kang for her input in our stochastic simulations, and J. Bellman and K. Noh for technical assistance.

This work was supported by Department of Interior grant No. D12AP00005 and the Charles Phelps Taft Research Center, University of Cincinnati.

REFERENCES

1. Dunlap, J. C. 1999. Molecular bases for circadian clocks. *Cell.* 96:271–290.
2. Dunlap, J. C., J. J. Loros, …, R. Lambreghts. 2007. A circadian clock in *Neurospora*: how genes and proteins cooperate to produce a sustained, entrainable, and compensated biological oscillator with a period of about a day. *Cold Spring Harb. Symp. Quant. Biol.* 72:57–68.
3. Baker, C. L., A. N. Kettenbach, …, J. C. Dunlap. 2009. Quantitative proteomics reveals a dynamic interactome and phase-specific phosphorylation in the *Neurospora* circadian clock. *Mol. Cell.* 34:354–363.
4. Cheng, P., Y. Yang, …, Y. Liu. 2001. Coiled-coil domain-mediated FRQ-FRQ interaction is essential for its circadian clock function in *Neurospora*. *EMBO J.* 20:101–108.
5. Crosthwaite, S. K., J. C. Dunlap, and J. J. Loros. 1997. *Neurospora* wc-1 and wc-2: transcription, photoresponses, and the origins of circadian rhythmicity. *Science.* 276:763–769.
6. Cheng, P., Y. Yang, and Y. Liu. 2001. Interlocked feedback loops contribute to the robustness of the *Neurospora* circadian clock. *Proc. Natl. Acad. Sci. USA.* 98:7408–7413.
7. Denault, D. L., J. J. Loros, and J. C. Dunlap. 2001. WC-2 mediates WC-1-FRQ interaction within the PAS protein-linked circadian feedback loop of *Neurospora*. *EMBO J.* 20:109–117.
8. Cheng, P., Q. He, …, Y. Liu. 2005. Regulation of the *Neurospora* circadian clock by an RNA helicase. *Genes Dev.* 19:234–241.
9. Cha, J., S. S. Chang, …, Y. Liu. 2008. Control of WHITE COLLAR localization by phosphorylation is a critical step in the circadian negative feedback process. *EMBO J.* 27:3246–3255.
10. Hong, C. I., P. Ruoff, …, J. C. Dunlap. 2008. Closing the circadian negative feedback loop: FRQ-dependent clearance of WC-1 from the nucleus. *Genes Dev.* 22:3196–3204.
11. Schafmeier, T., A. Diernfellner, …, M. Brunner. 2008. Circadian activity and abundance rhythms of the *Neurospora* clock transcription factor WCC associated with rapid nucleo-cytoplasmic shuttling. *Genes Dev.* 22:3397–3402.
12. Lee, K., J. J. Loros, and J. C. Dunlap. 2000. Interconnected feedback loops in the *Neurospora* circadian system. *Science.* 289:107–110.
13. Shi, M., M. Collett, …, J. C. Dunlap. 2010. FRQ-interacting RNA helicase mediates negative and positive feedback in the *Neurospora* circadian clock. *Genetics.* 184:351–361.
14. Lambreghts, R., M. Shi, …, J. J. Loros. 2009. A high-density single nucleotide polymorphism map for *Neurospora crassa*. *Genetics.* 181:767–781.
15. Sancar, G., C. Sancar, …, M. Brunner. 2011. A global circadian repressor controls antiphasic expression of metabolic genes in *Neurospora*. *Mol. Cell.* 44:687–697.
16. Sancar, G., C. Sancar, and M. Brunner. 2012. Metabolic compensation of the *Neurospora* clock by a glucose-dependent feedback of the circadian repressor CSP1 on the core oscillator. *Genes Dev.* 26:2435–2442.
17. Bugge, A., D. Feng, …, M. A. Lazar. 2012. Rev-erbα and Rev-erbβ coordinately protect the circadian clock and normal metabolic function. *Genes Dev.* 26:657–667.
18. Cho, H., X. Zhao, …, R. M. Evans. 2012. Regulation of circadian behavior and metabolism by REV-ERB-α and REV-ERB-β. *Nature.* 485:123–127.
19. Solt, L. A., Y. Wang, …, T. P. Burris. 2012. Regulation of circadian behavior and metabolism by synthetic REV-ERB agonists. *Nature.* 485:62–68.
20. Schafmeier, T., A. Haase, …, M. Brunner. 2005. Transcriptional feedback of *Neurospora* circadian clock gene by phosphorylation-dependent inactivation of its transcription factor. *Cell.* 122:235–246.
21. Kim, J. K., and D. B. Forger. 2012. A mechanism for robust circadian timekeeping via stoichiometric balance. *Mol. Syst. Biol.* 8:630.
22. Hong, C. I., I. W. Jolma, …, P. Ruoff. 2008. Simulating dark expressions and interactions of frq and wc-1 in the *Neurospora* circadian clock. *Biophys. J.* 94:1221–1232.
23. Ruoff, P., M. Vinsjevik, …, L. Rensing. 1999. The Goodwin oscillator: on the importance of degradation reactions in the circadian clock. *J. Biol. Rhythms.* 14:469–479.

24. Ruoff, P., J. J. Loros, and J. C. Dunlap. 2005. The relationship between FRQ-protein stability and temperature compensation in the *Neurospora* circadian clock. *Proc. Natl. Acad. Sci. USA.* 102:17681–17686.
25. Yu, Y., W. Dong, …, H. B. Schüttler. 2007. A genetic network for the clock of *Neurospora crassa*. *Proc. Natl. Acad. Sci. USA.* 104:2809–2814.
26. Garceau, N. Y., Y. Liu, …, J. C. Dunlap. 1997. Alternative initiation of translation and time-specific phosphorylation yield multiple forms of the essential clock protein FREQUENCY. *Cell.* 89:469–476.
27. Gonze, D., J. Halloy, and A. Goldbeter. 2002. Deterministic versus stochastic models for circadian rhythms. *J. Biol. Phys.* 28:637–653.
28. Gonze, D., W. Abou-Jaoudé, …, J. Halloy. 2011. How molecular should your molecular model be? On the level of molecular detail required to simulate biological networks in systems and synthetic biology. *Methods Enzymol.* 487:171–215.
29. Kim, J. K., K. Josić, and M. R. Bennett. 2014. The validity of quasi-steady-state approximations in discrete stochastic simulations. *Biophys. J.* 107:783–793.
30. Agarwal, A., R. Adams, …, H. Z. Shouval. 2012. On the precision of quasi steady state assumptions in stochastic dynamics. *J. Chem. Phys.* 137:044105.
31. Thomas, P., A. V. Straube, and R. Grima. 2012. The slow-scale linear noise approximation: an accurate, reduced stochastic description of biochemical networks under timescale separation conditions. *BMC Syst. Biol.* 6:39.
32. Kampen, N. G. v. 1992. Stochastic Processes in Physics and Chemistry. North-Holland, Amsterdam, Netherlands.
33. Gillespie, D. T. 1976. General method for numerically simulating stochastic time evolution of coupled chemical-reactions. *J. Comput. Phys.* 22:403–434.
34. Gillespie, D. T. 2007. Stochastic simulation of chemical kinetics. *Annu. Rev. Phys. Chem.* 58:35–55.
35. Chen, C. H., B. S. DeMay, …, J. J. Loros. 2010. Physical interaction between VIVID and white collar complex regulates photoadaptation in *Neurospora*. *Proc. Natl. Acad. Sci. USA.* 107:16715–16720.
36. Gooch, V. D., A. Mehra, …, J. C. Dunlap. 2008. Fully codon-optimized luciferase uncovers novel temperature characteristics of the *Neurospora* clock. *Eukaryot. Cell.* 7:28–37.
37. Hong, C. I., J. Zámborszky, …, A. Csikász-Nagy. 2014. Circadian rhythms synchronize mitosis in *Neurospora crassa*. *Proc. Natl. Acad. Sci. USA.* 111:1397–1402.
38. Dunlap, J. C., and J. J. Loros. 2005. Analysis of circadian rhythms in *Neurospora*: overview of assays and genetic and molecular biological manipulation. *Methods Enzymol.* 393:3–22.
39. Giles, N. H., M. E. Case, …, B. Tyler. 1985. Gene organization and regulation in the QA (quinic acid) gene cluster of *Neurospora crassa*. *Microbiol. Rev.* 49:338–358.
40. Aronson, B. D., K. A. Johnson, …, J. C. Dunlap. 1994. Negative feedback defining a circadian clock: autoregulation of the clock gene frequency. *Science.* 263:1578–1584.
41. Gardner, G. F., and J. F. Feldman. 1981. Temperature compensation of circadian period length in clock mutants of *Neurospora crassa*. *Plant Physiol.* 68:1244–1248.
42. Aronson, B. D., K. A. Johnson, and J. C. Dunlap. 1994. Circadian clock locus frequency: protein encoded by a single open reading frame defines period length and temperature compensation. *Proc. Natl. Acad. Sci. USA.* 91:7683–7687.
43. Liu, Y., J. Loros, and J. C. Dunlap. 2000. Phosphorylation of the *Neurospora* clock protein FREQUENCY determines its degradation rate and strongly influences the period length of the circadian clock. *Proc. Natl. Acad. Sci. USA.* 97:234–239.
44. Ruoff, P., S. Mohsenzadeh, and L. Rensing. 1996. Circadian rhythms and protein turnover: the effect of temperature on the period lengths of clock mutants simulated by the Goodwin oscillator. *Naturwissenschaften.* 83:514–517.
45. Gonze, D., and A. Goldbeter. 2006. Circadian rhythms and molecular noise. *Chaos.* 16:026110.
46. Bell-Pedersen, D., V. M. Cassone, …, M. J. Zoran. 2005. Circadian rhythms from multiple oscillators: lessons from diverse organisms. *Nat. Rev. Genet.* 6:544–556.
47. Stetson, M. H., and M. Watson-Whitmyre. 1976. Nucleus suprachiasmaticus: the biological clock in the hamster? *Science.* 191:197–199.
48. Kohsaka, A., A. D. Laposky, …, J. Bass. 2007. High-fat diet disrupts behavioral and molecular circadian rhythms in mice. *Cell Metab.* 6:414–421.
49. Tsai, T. Y., Y. S. Choi, …, J. E. Ferrell, Jr. 2008. Robust, tunable biological oscillations from interlinked positive and negative feedback loops. *Science.* 321:126–129.
50. Kim, J. K., Z. P. Kilpatrick, …, K. Josić. 2014. Molecular mechanisms that regulate the coupled period of the mammalian circadian clock. *Biophys. J.* 106:2071–2081.

Supporting Material

Mathematical Modeling and Validation of Glucose Compensation of the Neurospora Circadian Clock

Andrey A. Dovzhenok,[1] Mokryun Baek,[2] Sookkyung Lim,[1] and Christian I. Hong[2]*

[1]Department of Mathematical Sciences, University of Cincinnati, Cincinnati, Ohio;
and [2]Department of Molecular and Cellular Physiology, University of Cincinnati College of Medicine, Cincinnati, Ohio

*Correspondence: christian.hong@uc.edu

Table of contents

1. Supporting Text……...2

Text S1. Selection of Hill coefficients and other model assumptions …….2

Text S2. Regulation of clock period……..…….3

2. Supporting Figures……..6

3. Supporting Tables……..18

Table S1. Reactions and probabilities for the stochastic formulation of the model……...18

Supporting References……..20

1. SUPPORTING TEXT

Text S1. Selection of Hill coefficients and other model assumptions

It is known that stronger nonlinearity favors oscillations with a larger oscillatory domain (see, for example, (1)). Our simulations revealed that the increasing Hill coefficient of WC-1 activating *frq* produces larger period variations with the change in the *wc-1* transcription (k_7) or the WC-1 translation (k_8) rate constants (Fig. S1, *A* and *B*). Higher cooperativity of WC-1 activation of *frq* transcription leads to stronger nonlinearity in the model that produces sharper and larger increases of FRQ_n levels (Fig. S1, *C* and *D*). This is a critical observation for understanding how increased cooperativity of WC-1 activation of *frq* transcription influences the period in the model since FRQ_n plays a major role in changing the period (see Fig. S10 and Text S2 for more details) that was observed in overexpression and glucose experiments (2, 3). Higher reaction order (r = 2) of FRQ_c positive feedback on WC-1 translation is likely as FRQ is known to form homodimers (4). This high cooperativity also increased the period change in the model, although this increase was moderate compared to the increase due to higher cooperativity of WC-1 activating *frq* transcription. Ultimately, we explored different reaction orders for the Hill type functions discussed above with the combination used in this study (see model equations) eventually producing the best fit to the existing experimental data with the lowest possible cooperativity.

In this study, a relatively high reaction order (n = 6) of WC-1 activation of *frq* transcription is essential to simulate the existing experimental data on period variation. This high reaction order may be necessary to compensate for the insufficient nonlinearity in the simplified model we considered in this paper. In particular, our model does not include various reported post-translational modifications and interactions of the core clock components. For example, it is still unclear what role the experimentally observed progressive phosphorylation of FRQ (5) or the coiled-coil domain-mediated FRQ-FRQ interaction (4) play in the Neurospora circadian clock. Furthermore, the peak of FRQ was estimated to lag behind the peak of *frq* mRNA by about 4-6 hours (5) which suggests a delay in FRQ translation. If incorporated in the model, these regulatory interactions may increase overall nonlinearity and allow lower reaction order/Hill coefficient of WC-1 activation of *frq* transcription. However, they would also make equations

considerably more complex and therefore we do not include these post-translational modifications in the current simplified Neurospora circadian clock model.

Likewise, experimental observations suggest some post-translational modifications/interactions during WC-1 binding at the *frq* promoter. For example, the time between the peaks of WC-1 and FRQ was estimated from experimental data to be around 12 h (6). As we mentioned earlier, the peak of *frq* mRNA was reported to precede the peak of FRQ protein by about 4-6 hours (5) which means that the peak of *frq* mRNA happens about 6-8 hours after the peak of WC-1. Hence, there is either a delayed binding of WC-1 at the *frq* promoter or the transcription of *frq* does not start immediately after binding of WC-1 at the aforementioned promoter. In any case, the exact origin of observed delay remains unknown.

One notable property of the model is that one-parameter period diagrams for expression and translation rate constants of either *frq* or *csp-1* have identical shapes (although the parameter range of the two diagrams may be different). This property also holds for expression and translation rate constants k_7/k_8 of *wc-1* when the rate of change of cytosolic WC-1 ($d[\text{WC-1}_c]/dt$) is linearly dependent on the concentration of *wc-1* mRNA (see model equations in (7)). In contrast, when WC-1_c synthesis shows saturation kinetics in *wc-1* mRNA (as we model it in the current study) the period with the increase in parameter k_7 levels off at around 20 h and the period diagram is significantly different from the diagram in parameter k_8 (compare Fig. 4 *A* and Fig. S10 *A*). Our modeling results, experimental data on *wc-1* overexpression (2) and the fact that only decrease of the period was observed with the increase in glucose concentration in *csp-1*^{ko} strain (3) may indicate the existence of a *wc-1* mRNA saturation mechanism for WC-1 translation in Neurospora clock. Moreover, this modeling result also suggests that the increased abundance of WC-1 protein observed experimentally in *csp-1*^{ko} strains (3) is mainly due to the increased *wc-1* gene expression and not the increased translation rate.

Text S2. Regulation of clock period

A periodic solution in the *wc-1* transcription rate constant k_7 in the simulated *csp-1*^{ko} strain appears from the Hopf bifurcation (Fig. 4, *B* and *C*). However, the oscillatory range is unbounded from above due to saturation of WC-1 accumulation w.r.t. *wc-1* mRNA that we include in our model (see model equations). In contrast to the diagram in the rate constant k_7, the oscillatory region in the rate constant k_8 is bounded by the two Hopf bifurcations (Fig. S10, *B*

and *C*). Clock period in a close vicinity of the Hopf bifurcations follows the change in the amplitudes of FRQ_n or WC-1_n (Fig. S10). The same relationship between period and amplitude is observed in the model during initial period increase in the *wc-1* overexpression experiment in the *wc-1*^{ko} strain (Fig. 3 *C*) and during period decrease observed in the *csp-1* overexpression simulations (Figs. 3 *D* and S5 *A*). The characteristic feature of all these oscillatory regimes is low abundance of FRQ_n (Figs. 4B, S3 *B*, S5 *B* and S10 *B*) that is not sufficient to fully inactivate WC-1_n. This leads to low amplitude of WC-1_n oscillations (Figs. 4 *C*, S5 *C* and S10 *C*). In contrast, period changes away from the Hopf bifurcation points are almost inversely related to changes in the amplitude of FRQ_n (Fig. S10, *A* and *B*), although this correlation is not perfect as other variables also influence the period in the model. In contrast to FRQ_n, WC-1_n amplitude does not have an apparent relationship with the period away from the two Hopf bifurcations (Figs. 4 *C* and S10 *C*). Therefore, the vertical dashed lines in Fig. S10 that mark the peaks in the period curves may be considered the boundaries between the FRQ_n-regulated regime away from the Hopf bifurcations and low-amplitude regime in the vicinity of the Hopf bifurcations.

To explain the mechanism of how FRQ_n regulates the period in the model we turn to oscillatory profiles of WC-1_n and FRQ_n. When the rate of WC-1 translation (k_8) is relatively low it takes more time to accumulate WC-1 in the nucleus to start *frq* transcription and the period is long (Fig. S11 *A*). Increase in the WC-1 translation rate leads to faster accumulation of WC-1 in the nucleus and higher amplitude of WC-1_n oscillations (Fig. S11). High amplitude of WC-1_n oscillations triggers a sharp increase in *frq* mRNA abundance due to cooperativity of WC-1_n activation of *frq* transcription. This, in turn, results in rapid growth of the amplitude of FRQ_n oscillations and the accelerated clearance of WC-1 from the nucleus via complex formation with FRQ (Fig. S11 *B*). Faster WC-1 accumulation in the nucleus together with faster WC-1 clearance from the nucleus contribute to a dramatic decrease in the period when the parameter k_8 is moderately increased in the model (Fig. S11 *B*). Further increase in the rate of WC-1 translation results in an even higher WC-1_n amplitude (Figs. S10 *C* and S11 *C*). Since the model assumes degradation of WC-1_n (WCC) as a complex with FRQ_n (see model equations), the increasing WC-1_n abundance eventually starts to erode FRQ_n levels (Fig. S11, *C* and *D*). High abundance of WC-1_n and low abundance of FRQ_n lead to slower inactivation and removal of WC-1 from the nucleus (Fig. S11 *C*) and, ultimately, a longer period (Fig. S10 *A*).

Similar FRQ_n-regulated period change behavior is observed in the simulated WT strain after reinstatement of the negative feedback via *csp-1* in the model (Fig. S12). This result is expected because in both cases the increase in k_7 leads to higher abundance of WC-1 (Figs. 4 *C* and S12 *E*) which is the rate-limiting factor of the WCC and expression level of the WCC was found experimentally to determine the period of the circadian clock (2). In the *csp-1*^{ko} there is no inhibition of *wc-1* expression by CSP-1 and we simulate higher glucose levels by increasing parameter k_7 observing a decreased period (Fig. 4 *A*), as reported experimentally (3). In contrast, in the WT strain the glucose-dependent repression of *wc-1* transcription by CSP-1 counteracts increased expression of the *wc-1* gene at high glucose levels and the period remains constant (3).

2. SUPPORTING FIGURES

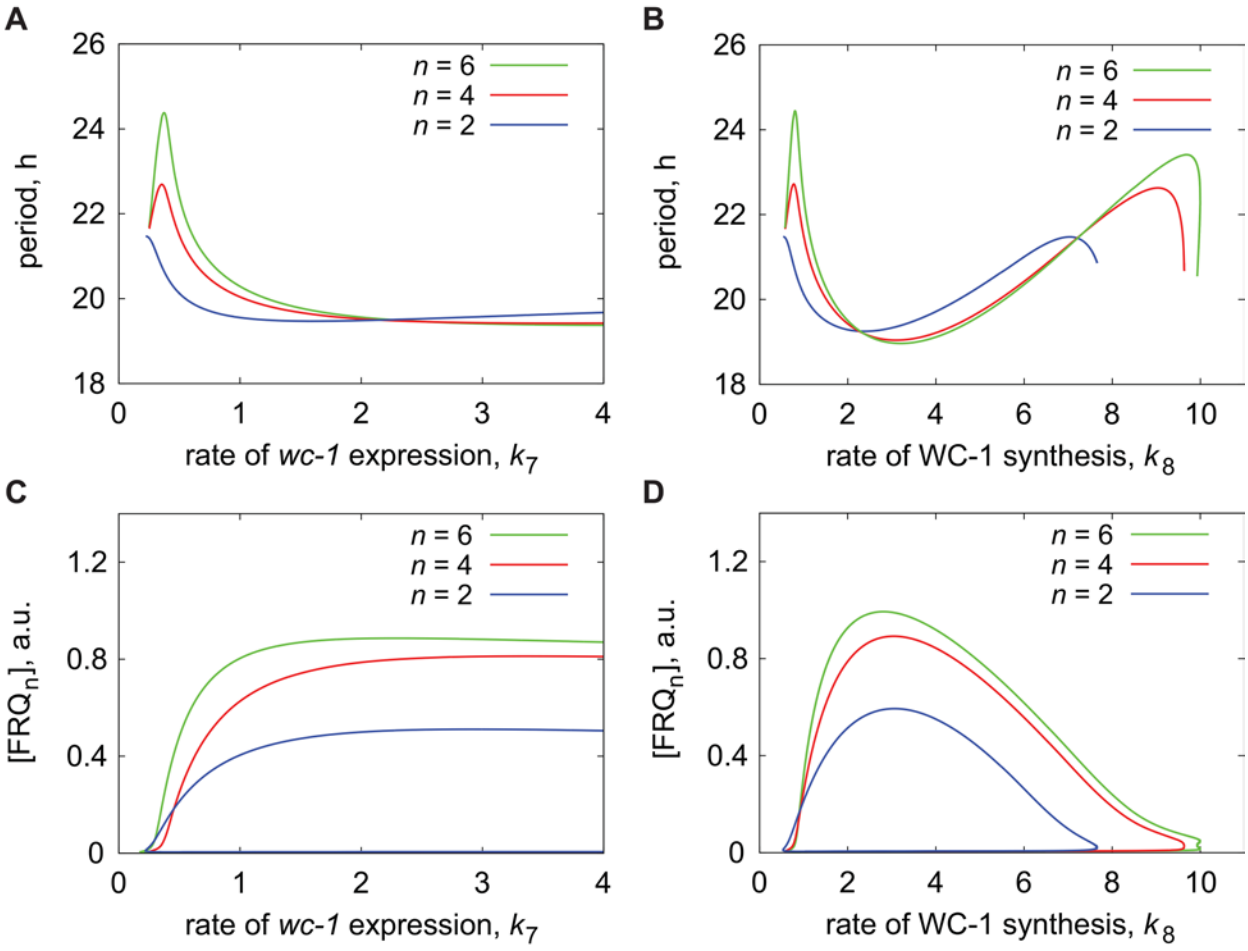

FIGURE S1 Period change and FRQ_n abundance with increasing Hill coefficient of WC-1 binding at the *frq* promoter. *(A)* Clock period and *(C)* envelope (max and min) of FRQ_n oscillations in the model with the increase of the *wc-1* expression rate constant k_7. *(B)* Clock period and *(D)* FRQ_n envelope (max and min) in the model with the increase of the WC-1 synthesis rate constant k_8. The Hill coefficient of WC-1 binding at the *frq* promoter is color coded (n = 2, 4 and 6).

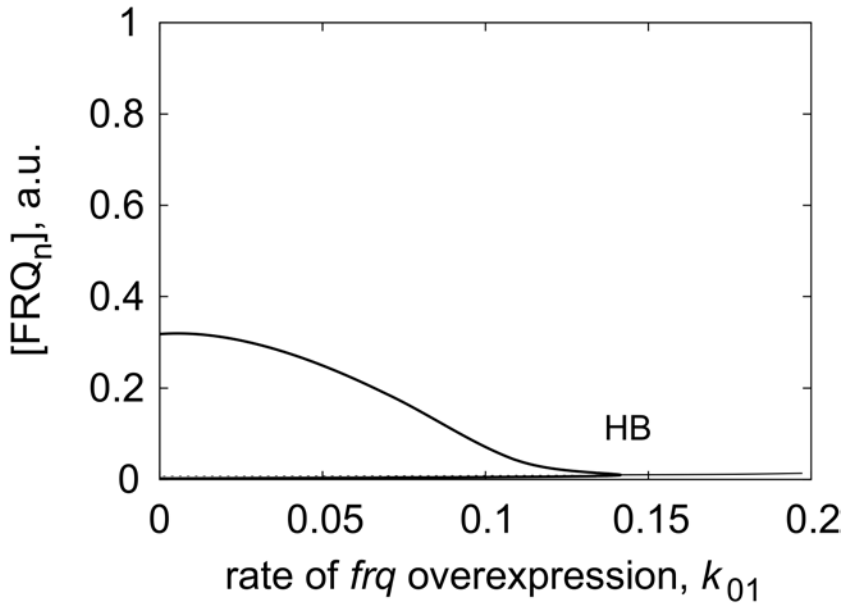

FIGURE S2 FRQ_n abundance in a simulated *frq* overexpression experiment in wild type genetic background. A bifurcation diagram showing the envelope (max and min) of FRQ_n oscillations (*thick solid curve*) as a function of the rate of *frq* overexpression, k_{01}. Oscillations disappear via a supercritical Hopf bifurcation (HB). The thin curve represents an unstable steady state. Parameter values are as described in Material and Methods.

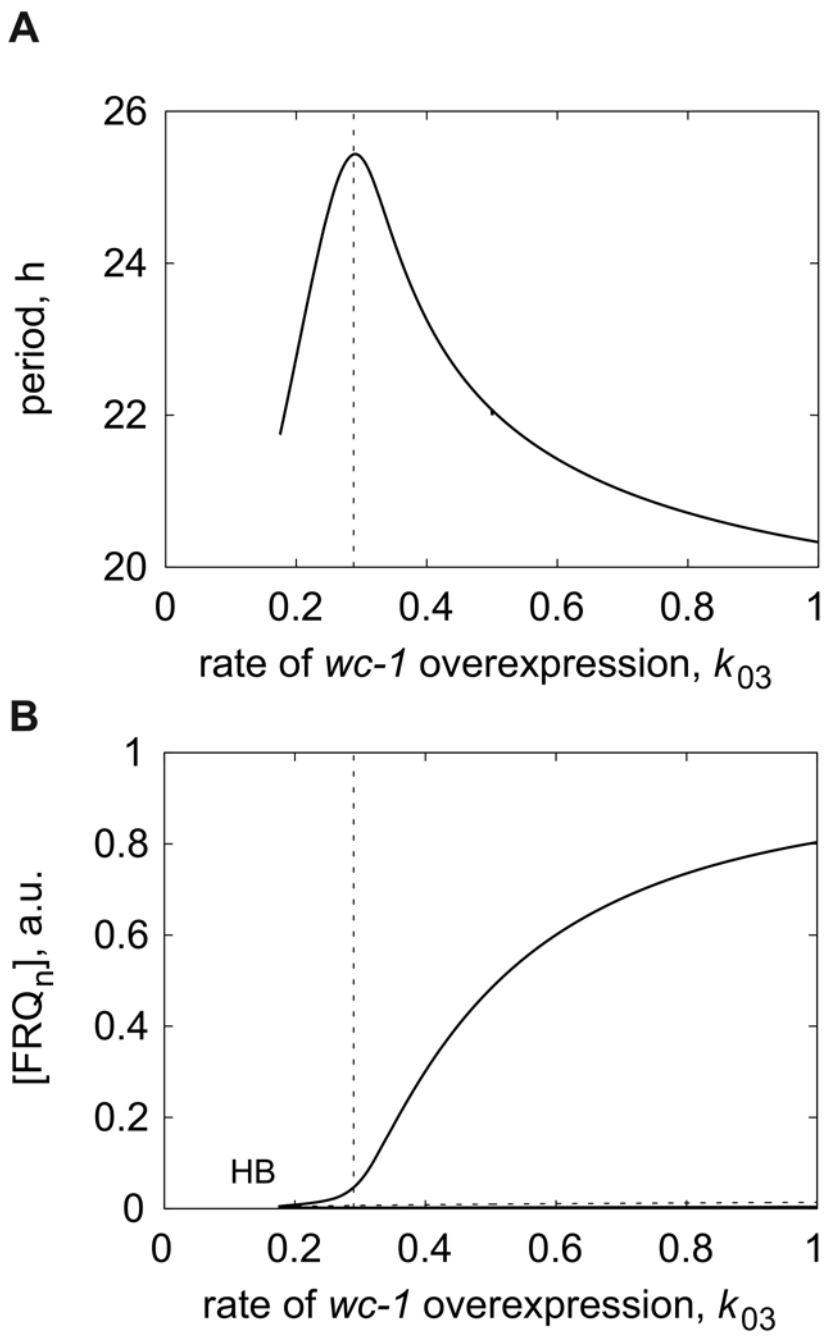

FIGURE S3 Clock period and FRQ_n abundance in a simulated *wc-1* overexpression experiment in *wc-1*^{ko} genetic background. *(A)* Period as a function of *wc-1* overexpression rate k_{03}. *(B)* A bifurcation diagram showing the envelope (max and min) of FRQ_n oscillations (*thick solid curve*) as a function of k_{03}. Oscillations appear via a supercritical Hopf bifurcation (HB). Dashed vertical lines mark the parameter value corresponding to the peak in the period curve in *(A)*. The thin dotted curve in *(B)* represents an unstable steady state. The *wc-1* expression rate constant $k_7 = 0$.

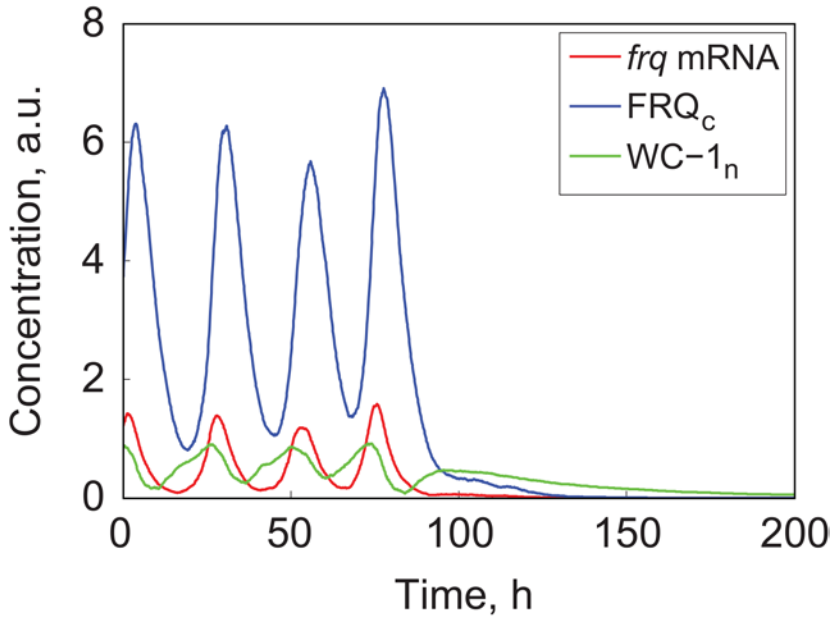

FIGURE S4 Die-out of oscillations in the stochastic version of the model in the presence of weak noise. When the circadian system is close to a Hopf bifurcation (Fig. S1), even a very weak noise may push the system into the basin of attraction of its co-existing steady state and oscillations would be lost. Time traces of *frq* mRNA, FRQ_c and $WC\text{-}1_n$ are shown. Parameter values are as described, except the *wc-1* expression rate constant $k_7 = 0$ and the *wc-1* overexpression rate $k_{03} = 0.26$. The volume factor of the stochastic simulations is $\Omega = 1000$.

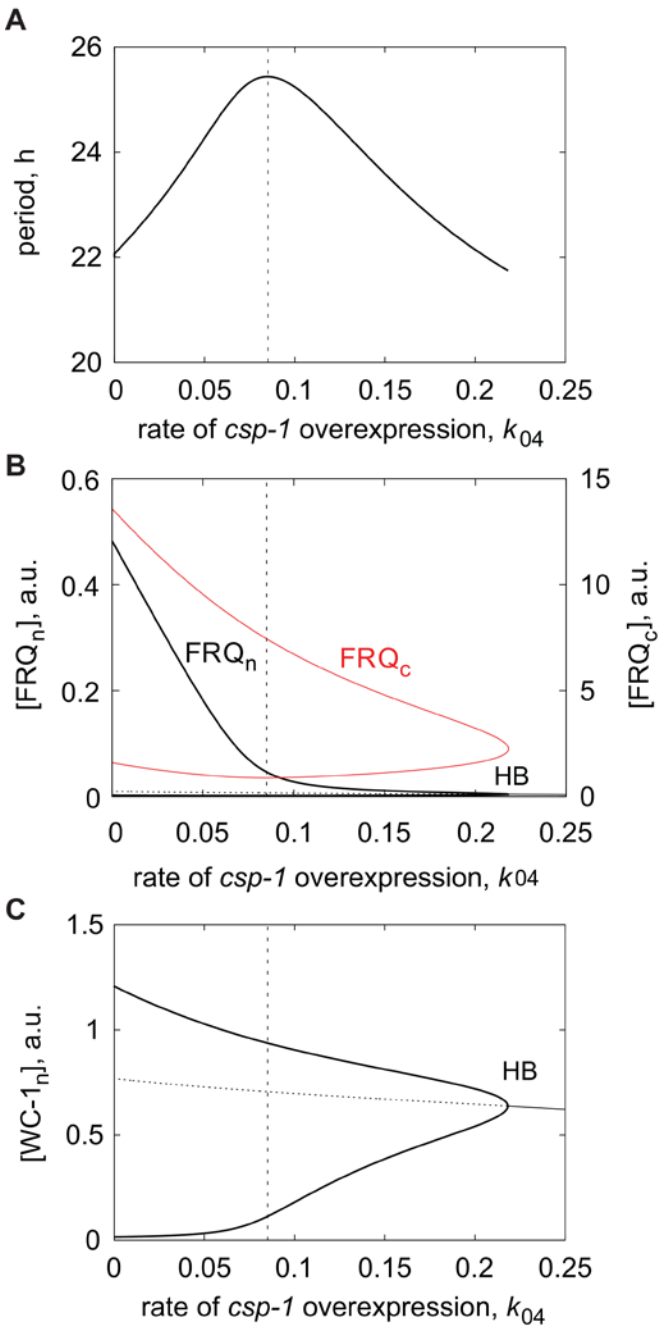

FIGURE S5 Period, FRQ_n and $WC\text{-}1_n$ levels in a simulated *csp-1* overexpression experiment. *(A)* Period as a function of the *csp-1* overexpression rate k_{04}. Bifurcation diagrams showing envelopes (max and min) of *(B)* FRQ_n (*black curve*) and FRQ_c (*red curve*) and *(C)* $WC\text{-}1_n$ oscillations (*thick solid curve*) as a function of k_{04}. Oscillations are lost via a supercritical Hopf bifurcation (HB). Thin solid (dotted) curves represent stable (unstable) steady states. Dashed vertical lines mark the parameter value corresponding to the peak in the period curve in *(A)*. Parameter values are as described in Materials and Methods, except the *csp-1* expression rate constant $k_{16} = 0$.

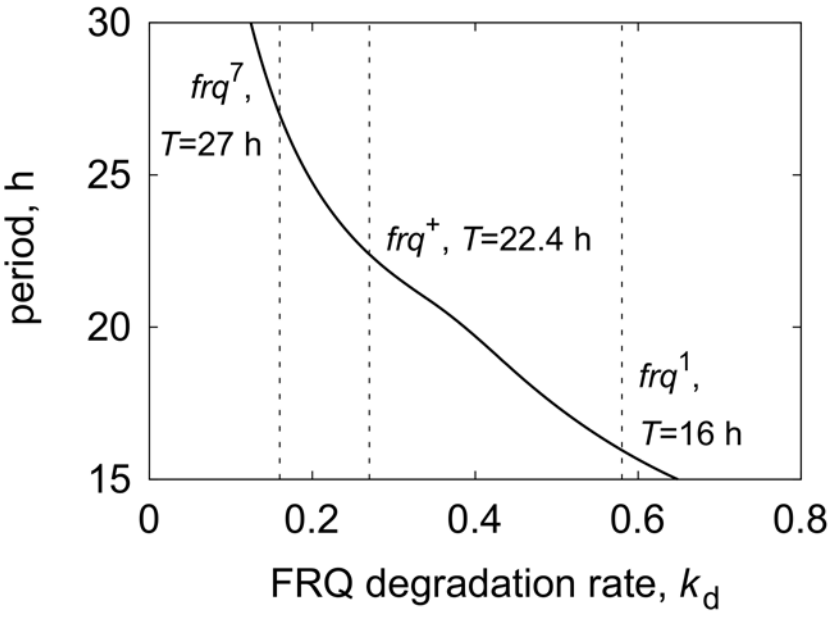

FIGURE S6 FRQ mutant alleles as simulated with varying the FRQ degradation rate. Vertical dashed lines mark FRQ degradation rate values corresponding to frq^7, frq^+ and frq^1 alleles as shown. The FRQ degradation rate k_d is defined as the rate of degradation of cytosolic and nuclear FRQ.

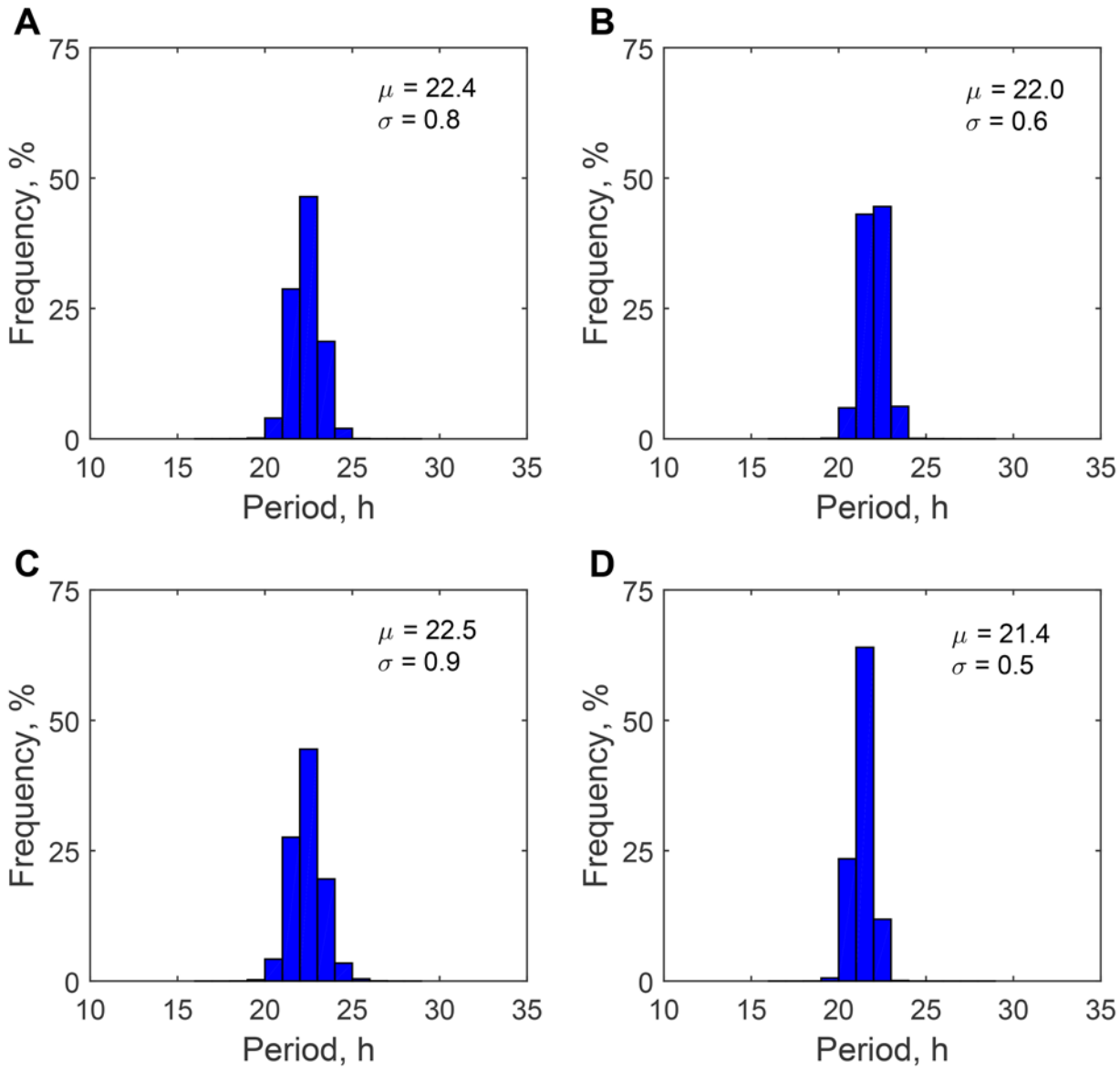

FIGURE S7 Histograms of period distributions obtained by stochastic simulations with weak noise. Period distributions in the presence of weak noise for the WT *(A, C)* and the *csp-1*^{ko} *(B, D)* in low and high glucose conditions, correspondingly. The histograms of periods of 10,000 cycles are computed from 100 simulation runs with 100 successive cycles with the volume factor Ω = 1000. The period was determined as the time interval separating two successive peaks of FRQ_c. The mean value (μ) and standard deviation (σ) of the period (in hours) is shown in each histogram. Parameter values are as described, except *(B)* $k_{16} = 0$, *(C)* $k_7 = 0.6$, $k_{16} = 0.57$ and *(D)* $k_7 = 0.6$, $k_{16} = 0$.

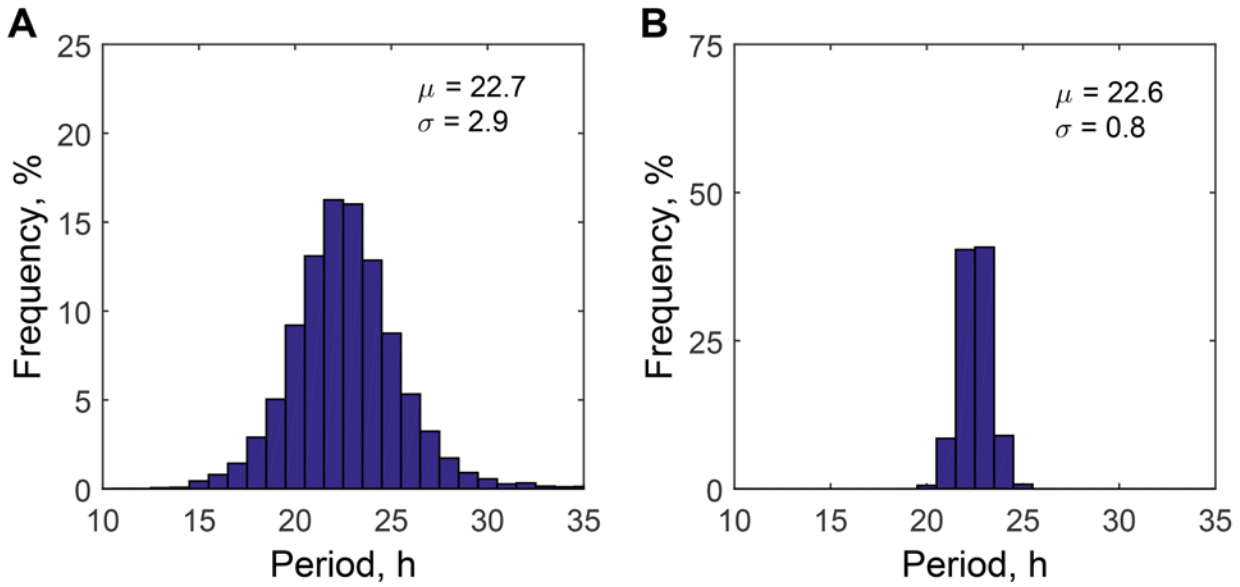

FIGURE S8 Histograms of period distributions obtained by stochastic simulations in a *csp-1*^{ko} parameter set in very low glucose. Period distributions in a *csp-1*^{ko} parameter set in very low glucose conditions in the presence of strong *(A)* or weak *(B)* noise. The histograms of periods of 10,000 cycles are computed from 100 simulation runs with 100 successive cycles with volume factors Ω = 100 *(A)* and Ω = 1000 *(B)*. The period was determined as the time interval separating two successive peaks of FRQ_c. The mean value (μ) and standard deviation (σ) of the period (in hours) is shown in each histogram. Parameter values are as described, except k_7 = 0.45, k_{16} = 0.

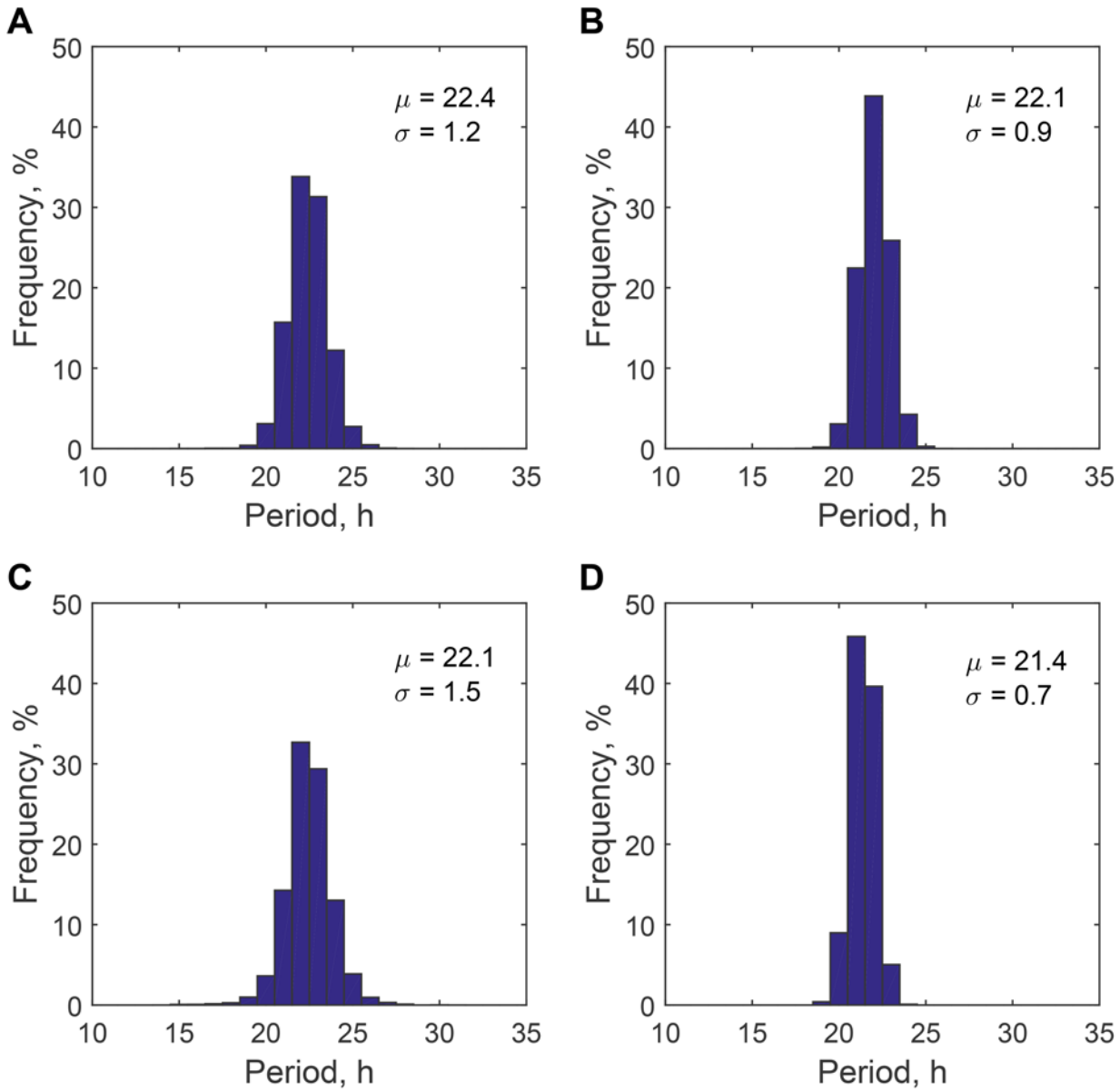

FIGURE S9 Histograms of period distributions obtained by rewriting the model equations as Langevin-type equations with multiplicative noise. Period distributions for the WT *(A, C)* and *csp-1*^{ko} *(B, D)* in low and high glucose conditions, correspondingly. Langevin-type equations have the form $dx_i/dt = f_i(...) + w_i(t)\sqrt{2D_i x_i}$, where $dx_i/dt = f_i(...)$ is the original deterministic equation, $w_i(t)$ is Gaussian white noise with zero mean and unit variance and $D_i = 0.0005$ is the noise amplitude that we kept the same for all variables. The histograms of periods of 10,000 cycles computed from 10 simulation runs with 1,000 successive cycles. The period was determined as the time interval separating two successive peaks of FRQ_c. The mean value (μ) and standard deviation (σ) of the period (in hours) is shown in each histogram. We obtain qualitatively similar results with the additive noise (not shown). Parameter values are as described, except *(B)* $k_{16} = 0$, *(C)* $k_7 = 0.6$, $k_{16} = 0.57$ and *(D)* $k_7 = 0.6$, $k_{16} = 0$.

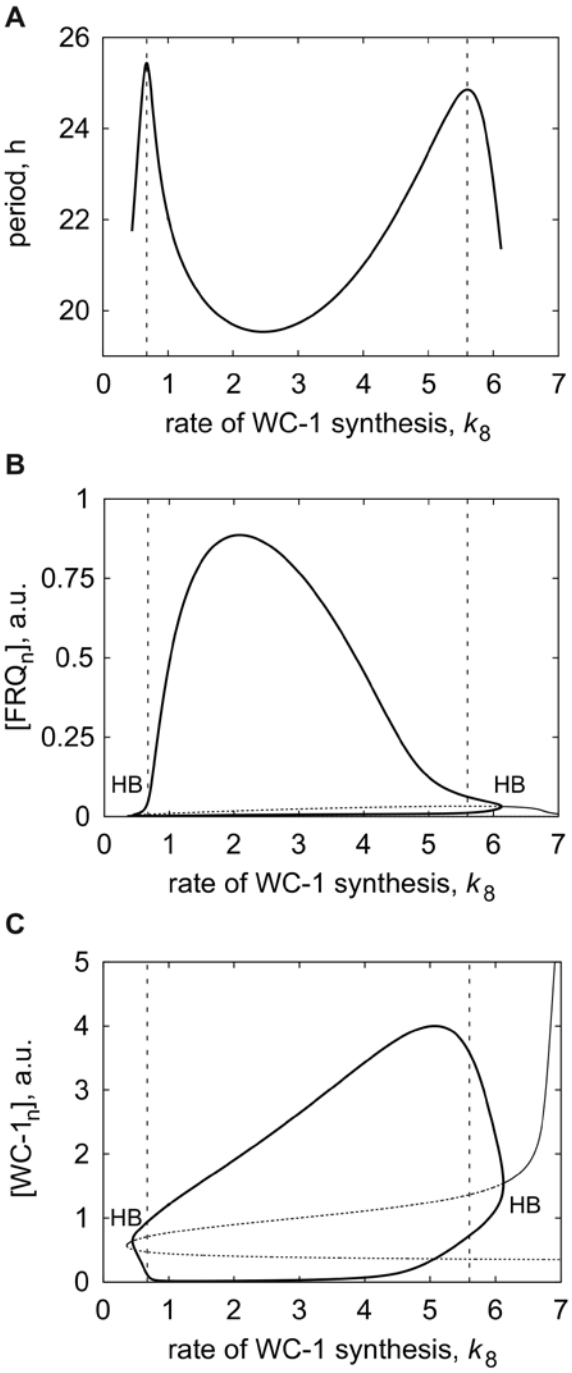

FIGURE S10 Clock period, FRQ_n and $WC\text{-}1_n$ levels in the *csp-1*^{ko} strain as a function of the WC-1 synthesis rate k_8. *(A)* The period as a function of k_8, simulating the increase in glucose concentration. One-parameter bifurcation diagrams show the envelopes (max and min) of *(B)* FRQ_n and *(C)* $WC\text{-}1_n$ oscillations (*thick solid curve*) as a function of k_8. Oscillatory regions are bounded by supercritical Hopf bifurcations (HB). Thin solid (dotted) curves represent stable (unstable) steady states. Dashed vertical lines mark the parameter values corresponding to the peaks in the period curve in *(A)*. Parameter values are as described, except $k_{16} = 0$.

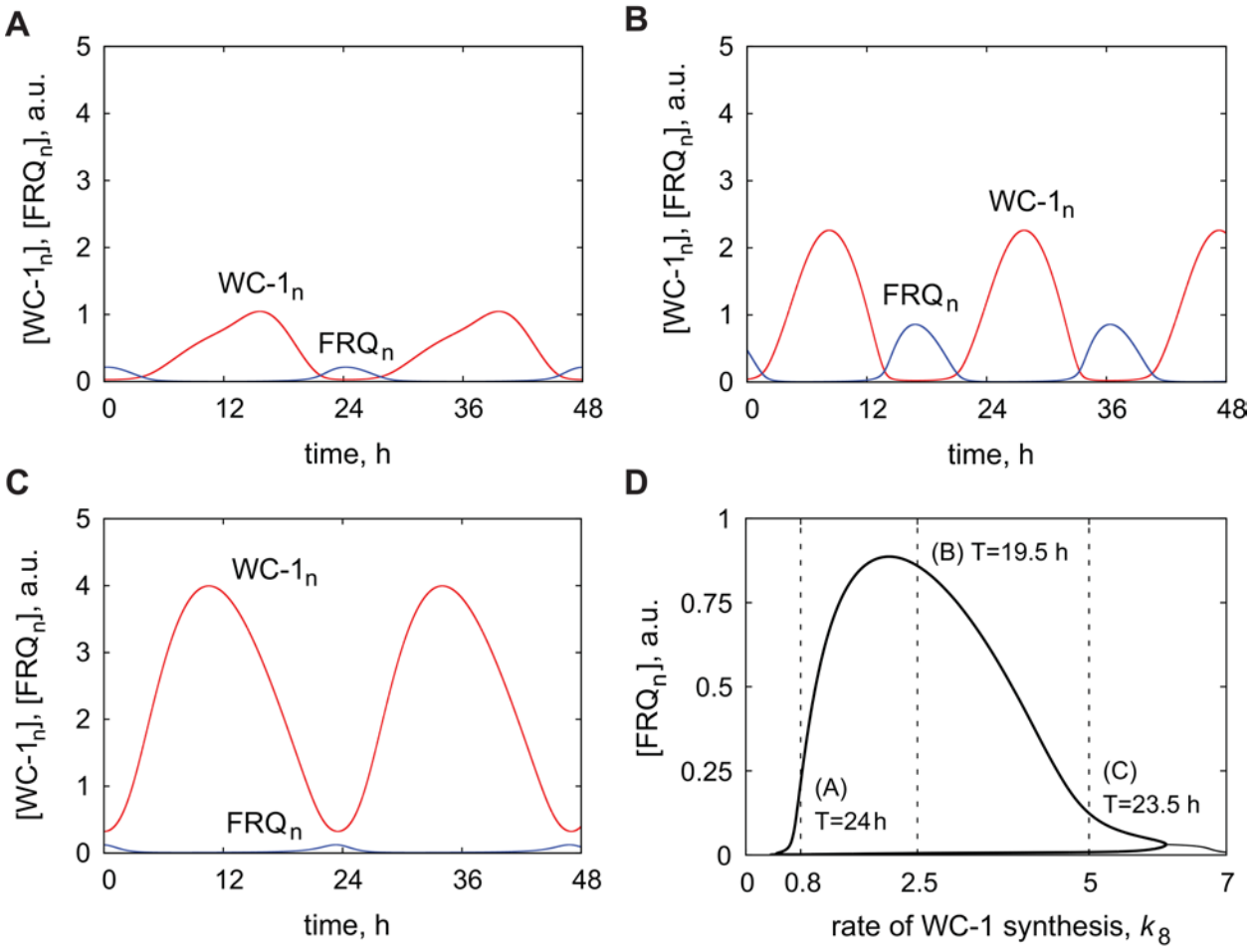

FIGURE S11 Oscillatory profiles of FRQ_n and $WC\text{-}1_n$ levels in the *csp-1*^{ko} strain with the increase in the WC-1 translation rate, k_8. *(A-C)* Oscillatory profiles of FRQ_n and $WC\text{-}1_n$ at different values of the WC-1 translation rate, k_8. *(D)* A one-parameter bifurcation diagram showing a steady state level of FRQ_n (*thin solid curve*) and the envelope (max and min concentrations) of FRQ_n oscillations (*thick solid curve*) as a function of k_8. Dashed vertical lines mark the parameter values corresponding to oscillatory profiles in *(A-C)*. Circadian periods for oscillatory profiles in *(A-C)* are also given. Parameter values are as described, except the rate of *csp-1* expression, $k_{16} = 0$ and *(A)* $k_8 = 0.8$, *(B)* $k_8 = 2.5$, *(C)* $k_8 = 5$.

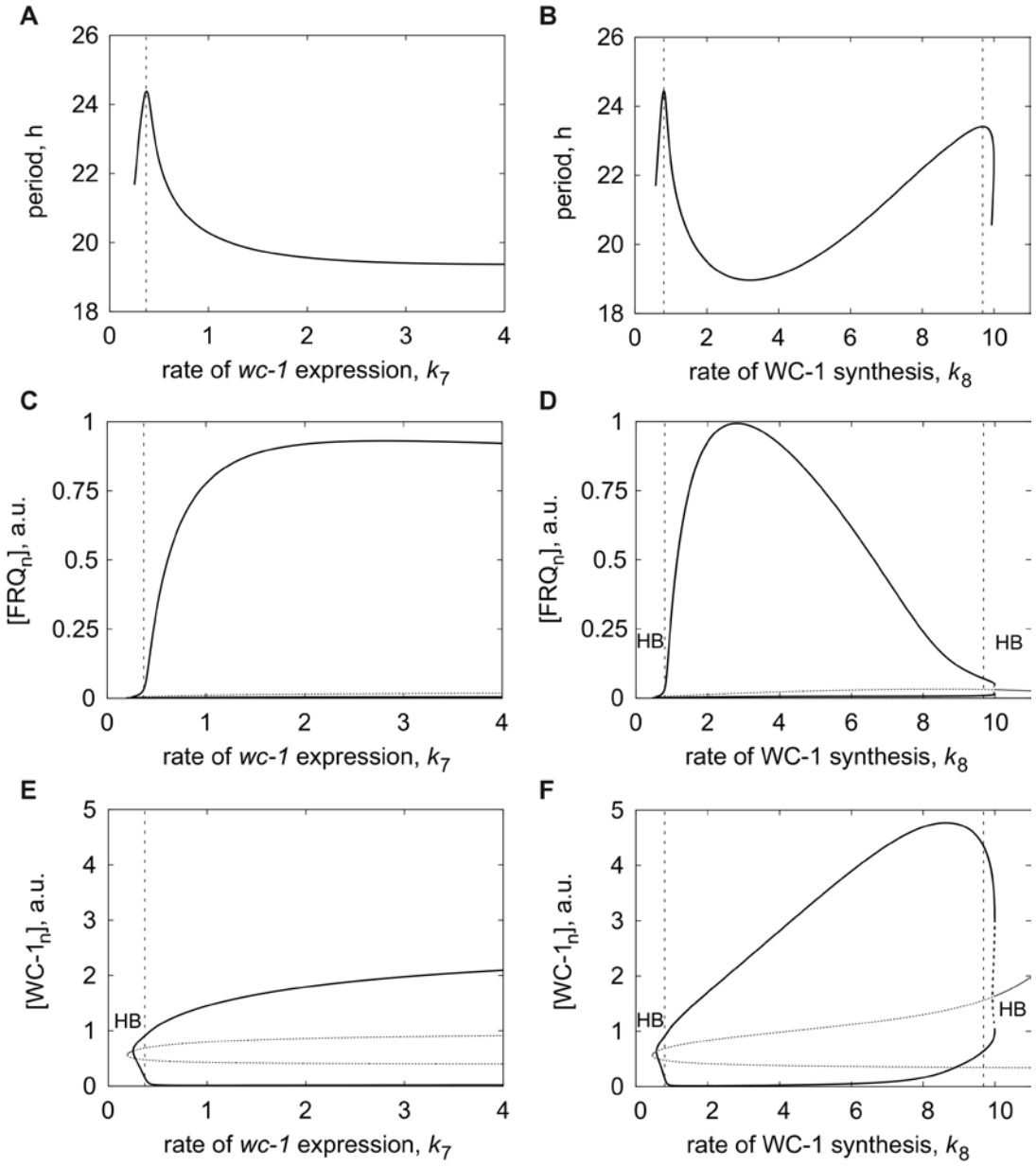

FIGURE S12 Simulated clock period, FRQ_n and $WC\text{-}1_n$ levels in the WT strain. *(A)* Clock period as a function of the *wc-1* expression rate constant k_7. *(B)* Clock period as a function of the WC-1 protein translation rate constant k_8. One-parameter bifurcation diagrams show the envelopes (max and min) of *(C)* FRQ_n and *(E)* $WC\text{-}1_n$ as a function of k_7. Oscillatory region in parameter k_7 is bounded by a supercritical Hopf bifurcation (HB) at the lower boundary. One-parameter bifurcation diagrams show the envelopes (max and min) of *(D)* FRQ_n and *(E)* $WC\text{-}1_n$ (*thick solid curve*) as a function of k_8. An oscillatory region in parameter k_8 is bounded by two supercritical Hopf bifurcations (HB). Dashed thick curves represent unstable oscillatory solutions, and thin solid (dotted) curves represent stable (unstable) steady states. Dashed vertical lines mark the parameter values corresponding to the peaks in the period curves in *(A)* and *(B)*.

3. SUPPORTING TABLES

TABLE S1 Reactions and probabilities for the stochastic formulation of the model. The second column provides the list of all reactions that occur in the model. The third column gives the probability of each reaction to occur. The change in the number of molecules as a result of a particular reaction is shown in the last column. G, H and I represent *frq*, *wc-1* and *csp-1* genes, correspondingly. Note that we do not decompose the terms of the deterministic model into detailed reaction steps.

Reaction number	Reaction	Probability of reaction	Transition
1	G $\rightarrow$ *frq* mRNA + G	$w_1 = (k_1\Omega)\dfrac{\text{WC-1}_\text{n}^{\,6}}{K\Omega^6 + \text{WC-1}_\text{n}^{\,6}}$	*frq* mRNA $\rightarrow$ *frq* mRNA + 1
2	*frq* mRNA $\rightarrow$	$w_2 = k_4 frq$ mRNA	*frq* mRNA $\rightarrow$ *frq* mRNA – 1
3	*frq* mRNA $\rightarrow$ FRQ_c + *frq* mRNA	$w_3 = k_2 frq$ mRNA	$\text{FRQ}_\text{c} \rightarrow \text{FRQ}_\text{c} + 1$
4	$\text{FRQ}_\text{c} \rightarrow \text{FRQ}_\text{n}$	$w_4 = k_3\text{FRQ}_\text{c}$	$\text{FRQ}_\text{c} \rightarrow \text{FRQ}_\text{c} - 1$ $\text{FRQ}_\text{n} \rightarrow \text{FRQ}_\text{n} + 1$
5	$\text{FRQ}_\text{c} \rightarrow$	$w_5 = k_5\text{FRQ}_\text{c}$	$\text{FRQ}_\text{c} \rightarrow \text{FRQ}_\text{c} - 1$
6	FRQ_n:$\text{WC-1}_\text{n} \rightarrow$ FRQ_n + WC-1_n	$w_6 = k_{14}\text{FRQ}_\text{n}$:$\text{WC-1}_\text{n}$	$\text{FRQ}_\text{n} \rightarrow \text{FRQ}_\text{n} + 1$ $\text{WC-1}_\text{n} \rightarrow \text{WC-1}_\text{n} + 1$ FRQ_n:$\text{WC-1}_\text{n} \rightarrow$ FRQ_n:$\text{WC-1}_\text{n} - 1$
7	$\text{FRQ}_\text{n} \rightarrow$	$w_7 = k_6\text{FRQ}_\text{n}$	$\text{FRQ}_\text{n} \rightarrow \text{FRQ}_\text{n} - 1$
8	FRQ_n + $\text{WC-1}_\text{n} \rightarrow$ FRQ_n:WC-1_n	$w_8 = (k_{13}/\Omega)\text{FRQ}_\text{n}\text{WC-1}_\text{n}$	$\text{FRQ}_\text{n} \rightarrow \text{FRQ}_\text{n} - 1$ $\text{WC-1}_\text{n} \rightarrow \text{WC-1}_\text{n} - 1$ FRQ_n:$\text{WC-1}_\text{n} \rightarrow$ FRQ_n:$\text{WC-1}_\text{n} + 1$
9	H $\rightarrow$ *wc-1* mRNA + H	$w_9 = (k_7\Omega)\dfrac{K_1\Omega}{K_1\Omega + \text{CSP-1}}$	*wc-1* mRNA $\rightarrow$ *wc-1* mRNA + 1
10	*wc-1* mRNA $\rightarrow$	$w_{10} = k_{10} wc\text{-}1$ mRNA	*wc-1* mRNA $\rightarrow$ *wc-1* mRNA – 1

11	*wc-1* mRNA → WC-1_c + *wc-1* mRNA	$w_{11} = (k_8\Omega)\frac{\text{FRQ}_\text{c}^{\,2}}{K_2\Omega^2 + \text{FRQ}_\text{c}^{\,2}} \cdot \frac{wc\text{-1 mRNA}}{K_3\Omega + wc\text{-1 mRNA}}$	WC-1_c → WC-1_c + 1
12	WC-1_c → WC-1_n	$w_{12} = k_9\text{WC-1}_\text{c}$	WC-1_c → WC-1_c – 1 WC-1_n → WC-1_n + 1
13	WC-1_c →	$w_{13} = k_{11}\text{WC-1}_\text{c}$	WC-1_c → WC-1_c – 1
14	WC-1_n →	$w_{14} = k_{12}\text{WC-1}_\text{n}$	WC-1_n → WC-1_n – 1
15	FRQ_n:WC-1_n →	$w_{15} = k_{15}\text{FRQ}_\text{n}$:$\text{WC-1}_\text{n}$	FRQ_n:WC-1_n → FRQ_n:WC-1_n – 1
16	I → *csp-1* mRNA + I	$w_{16} = k_{16}\text{WC-1}_\text{n}\frac{K_4\Omega}{K_4\Omega + \text{CSP-1}}$	*csp-1* mRNA → *csp-1* mRNA + 1
17	*csp-1* mRNA →	$w_{17} = k_{17}csp\text{-1 mRNA}$	*csp-1* mRNA → *csp-1* mRNA – 1
18	*csp-1* mRNA → CSP-1 + *csp-1* mRNA	$w_{18} = k_{18}csp\text{-1 mRNA}$	CSP-1 → CSP-1 + 1
19	CSP-1 →	$w_{19} = k_{19}\text{CSP-1}$	CSP-1 → CSP-1 – 1

SUPPORTING REFERENCES

1. Yu, Y., W. Dong, C. Altimus, X. Tang, J. Griffith, M. Morello, L. Dudek, J. Arnold, and H. B. Schuttler. 2007. A genetic network for the clock of Neurospora crassa. Proceedings of the National Academy of Sciences of the United States of America 104:2809-2814.
2. Cheng, P., Y. Yang, and Y. Liu. 2001. Interlocked feedback loops contribute to the robustness of the Neurospora circadian clock. Proceedings of the National Academy of Sciences of the United States of America 98:7408-7413.
3. Sancar, G., C. Sancar, and M. Brunner. 2012. Metabolic compensation of the Neurospora clock by a glucose-dependent feedback of the circadian repressor CSP1 on the core oscillator. Genes & development 26:2435-2442.
4. Cheng, P., Y. Yang, C. Heintzen, and Y. Liu. 2001. Coiled-coil domain-mediated FRQ-FRQ interaction is essential for its circadian clock function in Neurospora. The EMBO journal 20:101-108.
5. Garceau, N. Y., Y. Liu, J. J. Loros, and J. C. Dunlap. 1997. Alternative initiation of translation and time-specific phosphorylation yield multiple forms of the essential clock protein FREQUENCY. Cell 89:469-476.
6. Lee, K., J. J. Loros, and J. C. Dunlap. 2000. Interconnected feedback loops in the Neurospora circadian system. Science 289:107-110.
7. Hong, C. I., I. W. Jolma, J. J. Loros, J. C. Dunlap, and P. Ruoff. 2008. Simulating dark expressions and interactions of frq and wc-1 in the Neurospora circadian clock. Biophysical journal 94:1221-1232.